CHAPTER - 2

Conformational study of psychedelic (hallucinogenic) molecules: psilocybin, psilocin and mescaline

2.1 Introduction

Psilocybin and psilocin are the two main substances of magic mushrooms that, when consumed, are responsible to cause hallucinations in humans. Magic mushrooms include species of psilocybe like psilocybecubensis, psilocybemexicana, psilocybesubcubensis, psilocybesemilanceata, psilocybeargentipus etc. and occur naturally throughout the world.[1–3] These compounds were isolated and identified by Hofmann et al. in 1958.[4] Both psilocybin and psilocin have indole ring connected to an amino group by a 2 carbon side chain.[5,6] Their structural resemblance to the neurotransmitter serotonin leads to a profoundly hallucinogenic strength, as they disrupt the typical functions of brain serotonin.[7–9] Psilocybin shows a very interesting link with the cicada insects. It was reported that when massosporacicadina fungus infects cicada, psychoactive compounds gets produced among many other psychoactive compounds psilocybin was one of them present only in the infected cicadas.[10–13] Even though cicadas lose their abdomen due to the fungal infection yet they become hypersexual.[13,14] Though it is thought that psilocybin could act as an analgesic but its exact function in the infected cicadas remains yet to be understood.

Generally, psilocybin is considered as a pro drug whose active metabolite is psilocin. Psilocin is a dephosphorylated form of psilocybin. It is considered that the phosphate group acts as a protecting group for molecule until it reaches to its site of action.[15] It is reported that psilocybin is rapidly hydrolyzed to psilocin *in vivo*.[16] Psilocybin and psilocin both act as agonists or partial agonists at 5-hydroxytryptamine (5-HT)2A subtype receptors.[17–20]

Mostly psilocybin and psilocin have been studied as a novel therapeutic dug for many psychiatric disorders including major depression, obsessive compulsive disorder, anxiety and depression associated with life-threatening cancer and addiction.[21–27] The first synthetic psilocybin was produced in 1958 and continues to be widely used today.[17] In 1973 its crystal structure was studied by Weber et al.[15] Recently Sherwood et al. did phase

analysis of its crystal structure.[28] But an extensive conformational analysis of this molecule has not been carried out hitherto to the best of our knowledge.

One of the early molecular level studies on the conformation of psilocin was done by Cyrus et al.[29] where they drew similarity between psilocin and LSD besides conjecturing the possibility of intramolecular H-bonding between the nitrogen of ethyl amine chain and the indolic OH group for its hallucinogenic properties. Subsequently when T. J. Petcher et al.[15] elucidated the crystal structure of psilocin and precluded any possibility of intramolecular H-bonding although they mentioned that the crystal structure of psilocin was stabilized by intermolecular H-bonding. Since then there has been no detailed conformational analysis either experimentally or theoretically on psilocin.

Where psilocybin and psilocin belong to the family of indole alkyl amine compounds there is another psychedelic molecule that is mescaline which is a naturally occurring alkaloid that belongs to the phenylalkylamine family of compounds.[30] Despite its modest potency, mescaline has been referred to as a prototype hallucinogen because of its psychopharmacology, which is similar to that of other hallucinogens. It has a potency that is between 1000 and 3,000 times lower than LSD (lysergic acid diethylamide) and 30 times lower than psilocybin.[31–33]

It is predominantly found in various cacti, with notable sources including the Peyote cactus (Lophophora williamsii), the San Pedro cactus (Echinopsis pachanoi), as well as the Peruvian torch (Echinopsis peruviana), Bolivian torch (Echinopsis lageniformis), and Pereskia aculeate.[34,35] It can also be found in some members of the Fabaceae family, for instance, Acacia berlandieri.[36] Through radiocarbon dating, researches have estimated that mescaline was used for religious rituals and/or medical purposes some 5700 years ago, approximately.[37–39] In the context of North American legal system, although mescaline is a contraband, its use during religious ceremonies has been made legal since the 1920 in the Native American Church (NAC).[35,39,40] In 1896, Arthur Heffter who was the German chemist and pharmacologist successfully isolated mescaline for the first time.[41] In 1919, Ernst Spath, an Austrian chemist successfully synthesized the mescaline

by converting first 3,4,5-trimethoxybenzoic acid into its aldehyde form and then into final mescaline form.[42] With a greater affinity for the 5HT2A receptor (EC50 = 10M), mescaline functions as an agonist for the serotonin 2A/C (5HT2A/C) receptors. The adrenergic 2A receptor is another site of interaction.[30,43,44] Mescaline can cause an altered state of consciousness, which can include symptoms similar to those seen in schizophrenia. Mescaline's half-life is also longer than that of many other serotonin psychedelics. As a result of use of mescaline in naturalistic or religious settings, self-reported improvements in mental well-being and the ability to overcome alcoholism have been reported which indicate its therapeutic potentials.[45]

However, A better understanding of its potential clinical uses will require further research. And this warrants a thorough understanding of its molecular structure with all its conformations. In the latest study published by Taurian et al., the alkylamine side-chain conformation of phenylalkylamine, hallucinogen, was studied using ab initio methods,[46] but they did not examine all the parameters necessary to gauge the most stable conformer of mescaline.

As the conformation of a molecule plays a crucial role in determining its various properties, including physical, chemical, and biological aspects.[47,48] Hence, it is essential to gain a thorough understanding of these psychedelic molecules's conformational characteristics. By knowing the specific conformers and identifying its reactive centers, we can better comprehend their active involvement in both biological and physicochemical processes. It is well established that computational chemistry is efficient in structural elucidation and predicting the chemical properties of molecules as it provides a molecular level insight about geometrical properties, reaction pathways, and chemical mechanisms.[49,50] Hence, DFT method was used to extensively explore the conformational landscape and spectroscopic properties of these psychedelic molecules. The computational results of these psychedelic molecules reported in this work were found to be in exceedingly good agreement with the earlier reported experimental data.

2.2 Computational Details

Ground state optimization was done at B3LYP/cc-pVTZ level of theory for psilocybin, psilocin and mescaline molecules. For psilocybin Potential energy surface was generated with the step size 20° (containing 19 points) variation in all the dihedral angles such as C8-C15-C18-N21, C7-C8-C15-C18, C4-C3-O30-P31, H35-O33-P31-O30 [atom numbering as per figure 2.2] at the B3LYP/cc-pVTZ level of theory. Whereas for psilocin, a relaxed scan was performed to generate the potential energy surface at the B3LYP/cc-pVTZ level of theory with step size 5° variation in all the dihedral angles such as C23-N21-C18-H20, C2-C3-O30-H31, C8-C15-C18-N21 and C2-C8-C15-C18 [atom numbering as per figure 2.7]. While for mescaline a relaxed scan was performed to generate the potential energy surface at the B3LYP/cc-pVTZ level of theory with step size 5° variation in all the dihedral angles such as C6-C1-O19-C25, C1-C6-O18-C21, C1-C2-O20-C29, C5-C4-C9-C12 and C4-C9-C12-N15 [atom numbering as per figure 2.12]. Population of different conformers was calculated with the help of the following Boltzmann distribution equation:

$$N_f = \frac{e^{-\Delta E/RT}}{\sum_n e^{-\Delta E_n/RT}} \qquad (1)$$

Where, ΔE represents relative energy of a conformer with respect to global minimum structure and summation applied over the number of possible conformers (n).[51] For calculation R = 1.987 × 10^{-3} kcal.$K^{-1}$$mol^{-1}$ and T = 298 K was utilized.

To know about stability of molecules the Frontier molecular orbital (FMO) calculation was done. By utilizing FMO results the calculation of global reactivity descriptors like μ (Chemical potential), η (Chemical hardness), χ (Electronegativity) and ω (Electrophilicity index) were done with the help of equations as mentioned in introduction section 1.6.6.

Calculation of geometrical parameters and charge analysis were done at same level of theory. To find out the possible reactive centers in psilocybin, psilocin and mescaline molecules, the Electrostatic potential (ESP) mapping was carried out over optimized

structure of these molecules. Intramolecular charge transfer or electron delocalization, hyper-conjugative interactions and their strength in these psychedelic molecules have been investigated by natural bond order (NBO) calculation. The intramolecular (H-bond) interactions were investigated by means of Atoms in molecule (AIM) calculations and visualized utilizing Multiwfn software. TD-DFT[52] calculation was done to find out the maximum absorbance for these molecules. ^{1}H-NMR spectra was calculated using GIAO method.[53–57] Harmonic vibrational IR active modes were also calculated. All the above calculations were carried out at the B3LYP/cc-pVTZ for psilocybin, psilocin and at CCSD/cc-pVDZ level of theory for mescaline. These calculations were performed with the help of Gaussian 16 suite of program and for the assignment of vibrational modes Gaussview 6.0.1 software was utilized.

2.3 Results and Discussion

2.3.1a Conformational analysis of psilocybin

Weber et al. reported two conformers of psilocybin by analyzing the X-ray crystal structure of psilocybin.[15] A section of the conformational manifold of psilocybin was explored by computing the potential energy surface corresponding to the dihedral angles (C8-C15-C18-N21), (C7-C8-C15-C18), (C4-C3-O30-P31) and (H35-O33-P31-O30) carried out in steps of 20° of the 360° complete rotation around the bond at the B3LYP/cc-pVTZ level of theory through a relaxed scan (Figure 2.1). These relaxed scan revealed a global minimum (Figure 2.1(a)) in a shallow potential. Among several other local minima, the one with the second lowest energy was considered as the second conformer of psilocybin and named conformer-B whose energy was 2.08 kcal/mol higher than the global minimum. It must be noted that the starting configuration in other relaxed scans, shown in Figure 2.1 b, c and d, was the minimum in these scans identical to conformer-A. The scale in figure 2.1 is set from 0° to 360° dihedral angle where angle 0° in Figure 2.1(a) denotes 175.5° in the molecule. Similarly, 0° denotes -114.1° in figure 2.1(b) and 92.7° for figure 2.1(c), 125.4° in figure 2.1(d). Populations of conformer-A and conformer-B were further calculated using the Boltzmann distribution equation and the

results are summarized in table 2.1. From the table 2.1, it is evident that when the entire conformational space was explored by varying the C15-C18 bond, the conformer-A was observed to have maximum cumulative population (97.71%) followed by conformer-B. Harmonic frequency analysis of both these conformers had no imaginary frequencies. Therefore, for detailed structural and spectroscopic analysis of psilocybin both of these conformers A and B were chosen in this study. Figure 2.2, represents optimized geometry of both the conformers. The rotational barrier from conformer-A to conformer-B was calculated to be 14.63 kcal/mol. Such a large rotational barrier is due to the obvious steric repulsion between one of the alkyl group of ethyl amine and indole ring cavity in conformer-B, while no such repulsion was seen in conformer-A. Other possible conformers of psilocybin resulting from changing other dihedral angles were also explored and the resulting surfaces are shown in figure 2.3(a to d). It must be noted that the minima in all these surfaces are relatively higher in energy compared to the conformers A and B identified above.

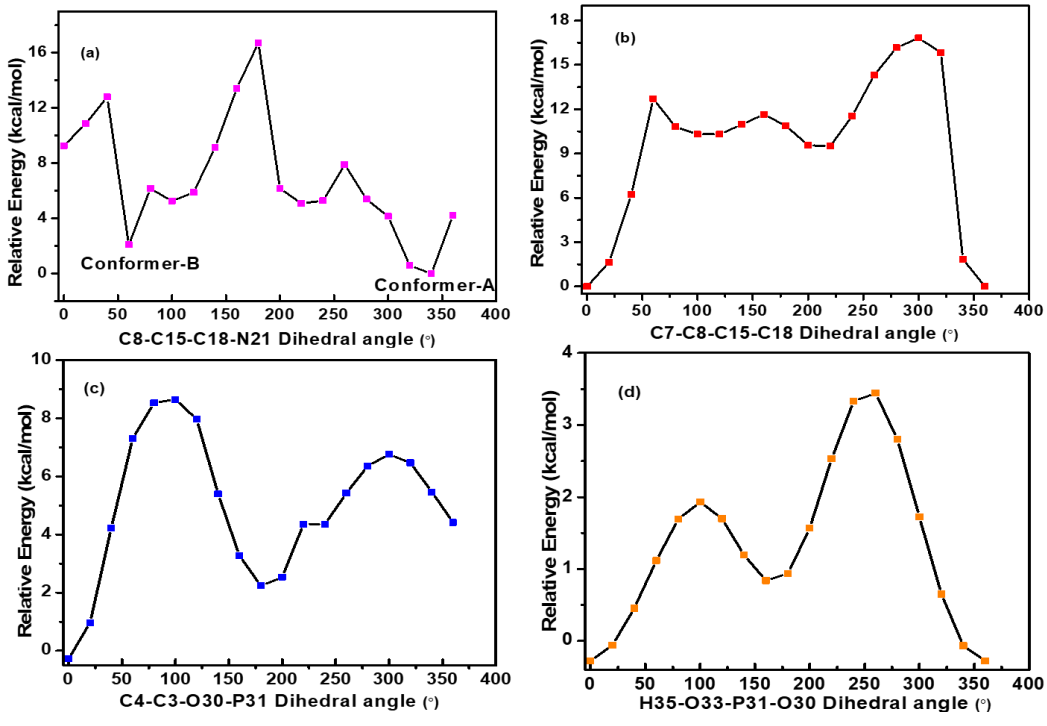

Figure 2.1: Dihedral angle-relative energy curve (a-d) of psilocybin at B3LYP/cc-pVTZ level of theory

Various computational methods were scanned to identify the best possible computational approach for an extensive study of this molecule and the result is shown in figure 2.4 where conformer-A's energy computed (optimized) at B3LYP/cc-pVTZ level of theory is taken as the reference and other values are depicted relative to it. It is evident from figure 2.4 that other than B3LYP/cc-pVTZ level of theory all other methods overestimate the energy values. Hence B3LYP/cc-pVTZ level of theory was considered to be the optimal one and therefore all subsequent structural and spectroscopic calculations were carried out using B3LYP/cc-pVTZ level of theory.

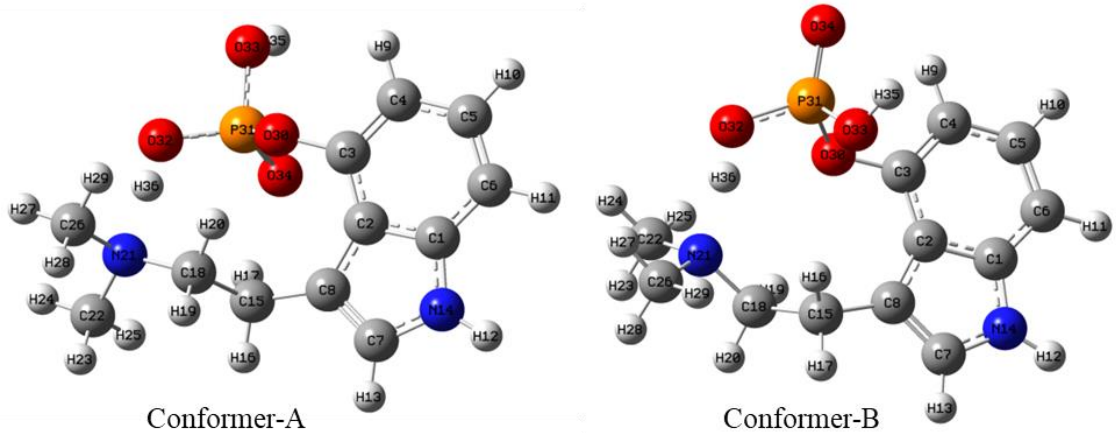

Figure 2.2: Optimized structures of Conformers A & B of psilocybin (numbers on atoms represent the label of that atom in the optimized geometry)

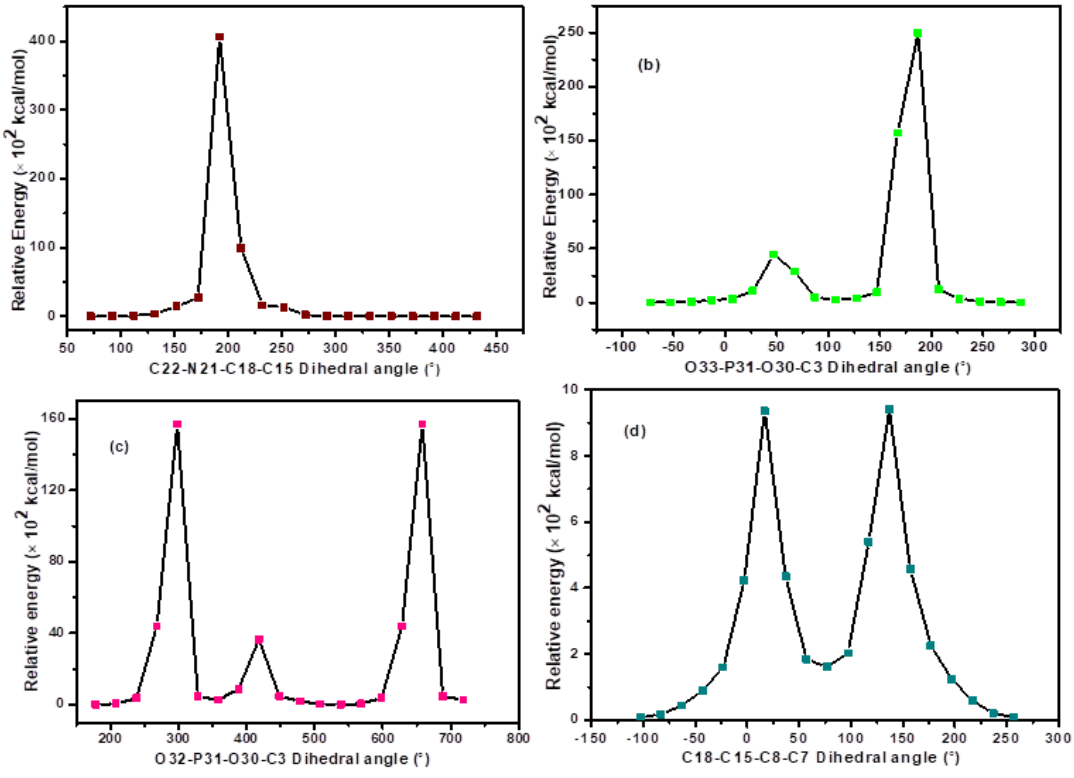

Figure 2.3: The a,b,c, and d curves are the Dihedral-relative energy curve of psilocybin molecule at B3LYP/cc-pVTZ level of theory

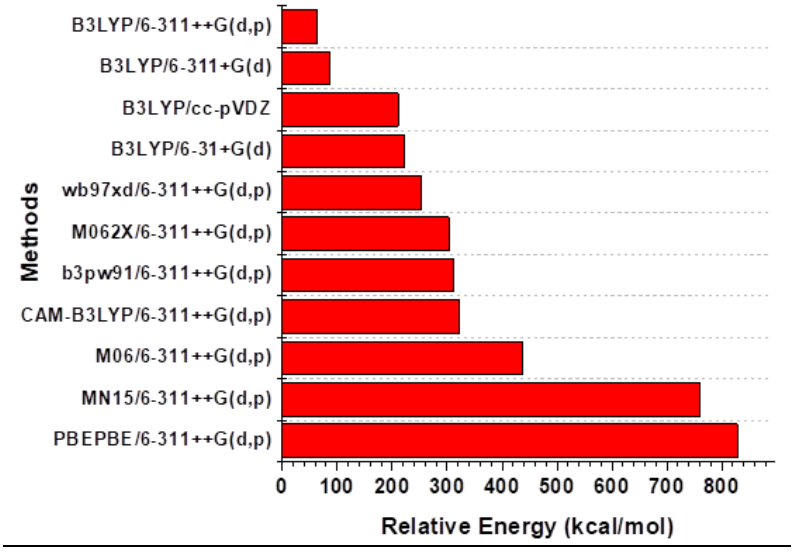

Figure 2.4: Plot of relative energy vs. methods

Table 2.1: Conformational abundance of the psilocybin molecule at B3LYP/cc-pVTZ level of theory

Dihedral angle [°]	C8-C15-C18-N21	
	ΔE [kcal/mol]	N_f [%]
0	9.27	0.00
20	10.84	0.00
40	12.79	0.00
60	2.08	2.10[Conformer-B]
80	6.16	0.00
100	5.25	0.01
120	5.86	0.00
140	9.14	0.00
160	13.42	0.00
180	16.72	0.00
200	6.16	0.00
220	5.08	0.01
240	5.27	0.01
260	7.88	0.00
280	5.37	0.01
300	4.14	0.06
320	0.57	26.76
340	0.00	70.95[Conformer-A]
360	4.19	0.05

Where, ΔE represents relative energy of a conformer with respect to global minimum structure; N_f is population of different conformers, calculated utilizing Boltzmann distribution equation which is given as equation (1).

2.3.1b Conformational analysis of psilocin

T. J. Petcher et al.[58] reported one conformer of psilocin by analyzing the X-ray crystal structure of psilocin. Herein conformers of psilocin molecule were explored by computing the potential energy surface corresponding to the dihedral angles (C23-N21-C18-H20), (C2-C3-O30-H31), (C8-C15-C18-N21) and (C2-C8-C15-C18) (Note that the number after the atomic symbol here as well as elsewhere represents the labeling scheme as per Figure 2.7). These dihedral angles were systematically varied in steps of 5° of the 360° complete rotation around the bond at the B3LYP/ccpVTZ level of theory through a relaxed scan (Figure 2.5 and Figure 2.6). In the individual relaxed scan of (C8-C15-C18-

N21) and (C2-C8-C15-C18) shown in figure 2.5(a) and 2.5(b)), it was observed that the initial geometry had the lowest energy. But when both these dihedral angles were scanned simultaneously at 20° intervals, one global minimum was observed (figure 2.5(c)). In the simultaneous relaxed scan of the other two dihedral angles i.e. (C23-N21-C18-H20) and (C2-C3-O30-H31), along with one global minimum another minimum was also observed, shown in figure 2.6(a). Further individual scans of both these dihedral revealed an explicit global minimum at 46.8° (for C23-N21-C18-H20) and another minimum at 182.3° (for C2-C3-O30-H31) dihedral angle which are shown in figure 2.6(b) and 2.6(c). Figure 2.6c is essentially the OH bond rotation and the barrier for the same was calculated to be 3.83 kcal/mol from this scan. The global minimum obtained from both the contour maps was designated as conformer-A and the second most stable conformer was designated as conformer-B. It is to be noted that the scale for figure 2.5 and figure 2.6 is set from 0° to 360° dihedral angle but in actual molecule the 0° denotes -178.6° for C8-C15-C18-N21 scan, 76.2° for C2-C8-C15-C18 scan while 171.8° for C23-N21-C18-H20 and 7.3° for C2-C3-O30-H31 dihedral scan.

The energy difference between Conformer-A and Conformer-B was calculated to be 5.4 kcal/mol. This calculated energy difference was further verified by carrying out population analysis. Harmonic frequency analysis of both the conformers had no imaginary frequencies. Therefore, for detailed structural and spectroscopic analysis of psilocin molecule both the conformers A and B were taken further. Figure 2.7, represents the optimized geometry of conformer-A and B. Besides, two other higher energy conformers were also observed in the relaxed scan of C23-N21-C18-H20 dihedral angle which are shown in figure 2.8. These are Conformer-C and Conformer-D obtained at 306.8° and 171.8° dihedral angle along with global minimum. Both these conformers were found to be 5.6 kcal/mol and 6.6 kcal/mol higher in energy than global minimum. In both These conformers there is no possibility of intra as well as intermolecular H-bond interaction because the H atom of O-H group is hindered therefore we did not consider these conformers for detailed analysis of psilocin molecule.

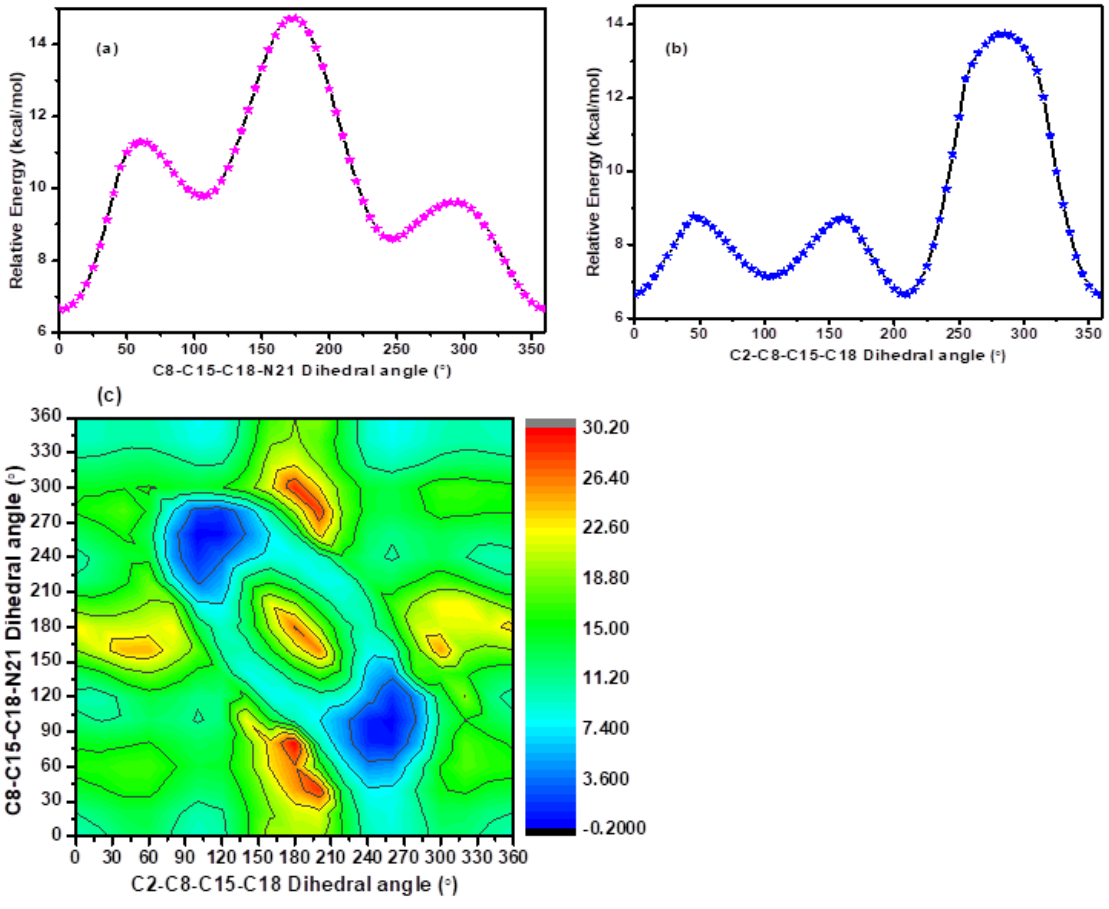

Figure 2.5: Potential energy curve [a (C15-C18 bond rotation) and b (C8-C15 bond rotation)] and Potential energy surface (c) for simultaneous rotation of C15-C18 and C8-C15 bond of psilocin molecule generated at B3LYP/cc-pVTZ level of theory. (Number after the atomic symbol represents the labeling scheme as per Figure 2.7).

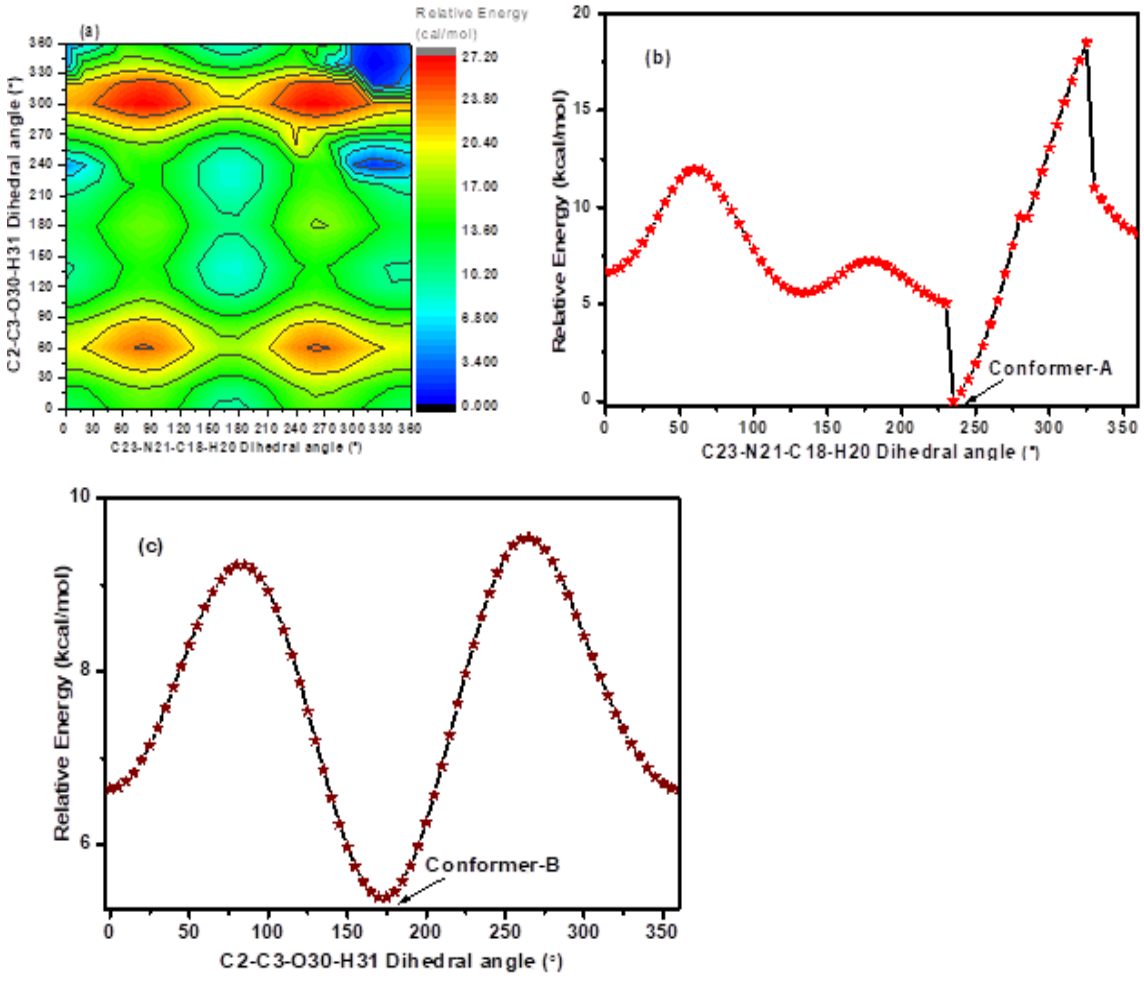

Figure 2.6: Potential energy surface (a) for simultaneous C3-O30 and N21-C18 bond rotation and potential energy curve (b) for N21-C18 and (c) for C3-O30 bond rotation generated at B3LYP/cc-pVTZ level of theory. (Number after the atomic symbol represents the labeling scheme as per Figure 2.7).

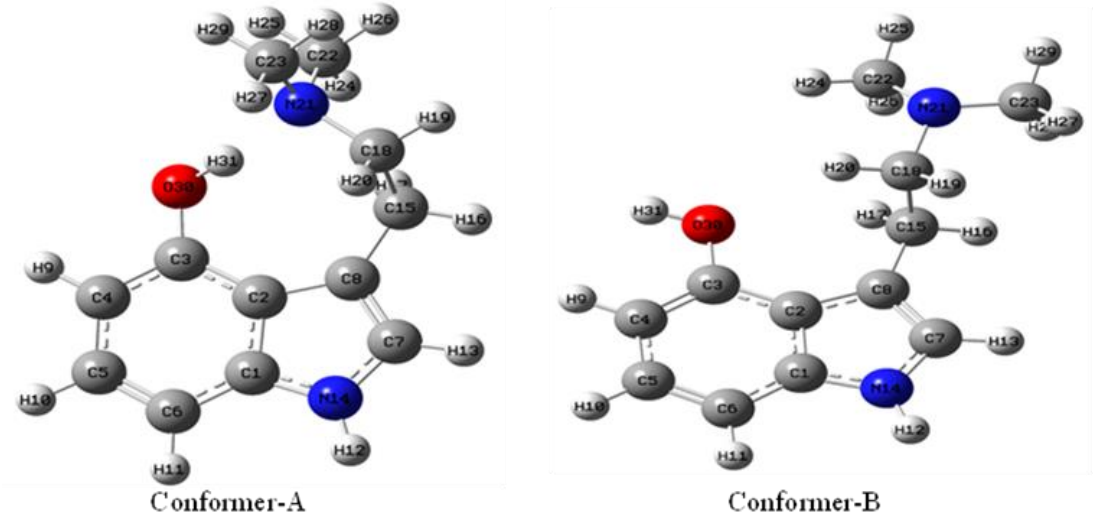

Figure 2.7: Optimized structures of both the conformers (A & B) of psilocin; where, numbers after atoms represent the label of that atom in optimized geometry

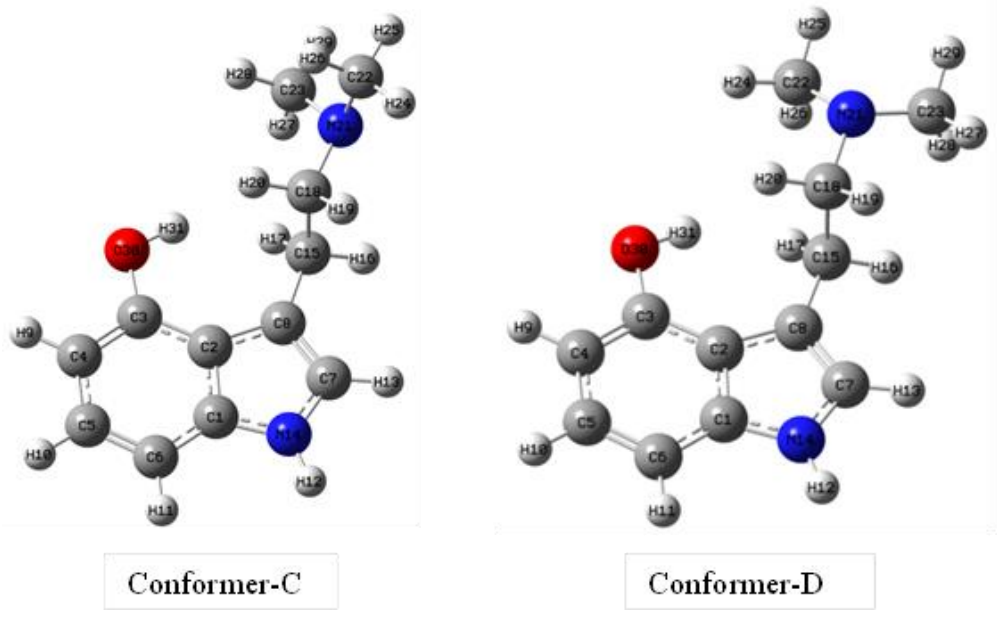

Figure 2.8: Structure of Conformer-C and Conformer-D

To identify the best possible computational approach various computational methods were examined, shown in figure 2.9, for an extensive study of psilocin molecule. It was found that the predictions made at B3LYP/cc-pVTZ with respect to the bond parameters

and normal modes of vibration matched relatively well with the experiments compared to the other methods that were tried. Therefore, this method was considered as the optimal and further calculations were made for psilocin using it.

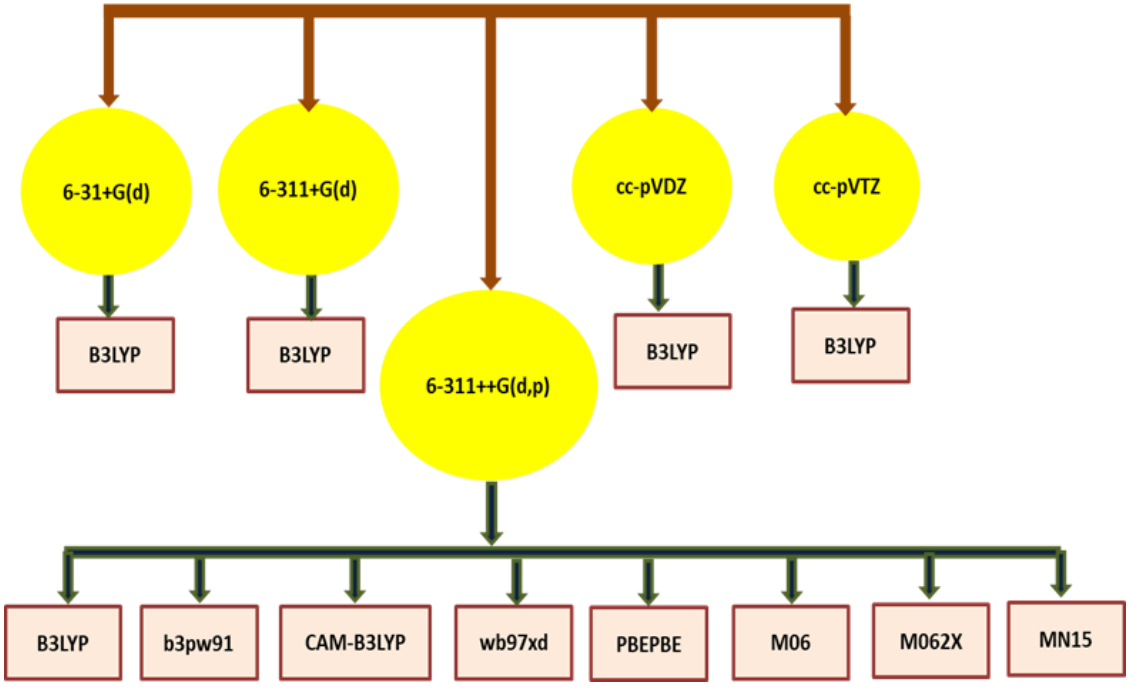

Figure 2.9: Optimization with functionals (in the rectangle) and basis sets (in the circle)

2.3.1c Conformational analysis of mescaline

S. R. Ernst et al. reported only one conformer of mescaline by analyzing the X-ray crystal structure of mescaline hydrobromide.[59] While a different conformer of mescaline was observed in its X-ray crystal structure by Tsoucaris et al. while studying mescaline hydrochloride.[60] In the backdrop of such contrasting experimental results, it is of paramount importance to access the structure of the most stable conformer. Hence the conformational space of mescaline was extensively explored by computing the potential energy surfaces corresponding to the dihedral angles (C4-C9-C12-N15) and (C1-C6-O18-C21), carried out in steps of 5° of the 360° complete rotation around the respective bonds at the B3LYP/cc-pVTZ level of theory through a relaxed scan (Figure 2.10).

The scale in figure 2.10 is set from dihedral angle 0° to 360° where angle 0° in figure 2.10(a) denotes -42.8° in the molecule. Similarly 0° denotes -178.5° in figure 2.10(b) and -177.6° in figure 2.10(c). From Figure 2.10 it is evident that scanning C1-C6-O18-C21 dihedral angle resulted in 2 minima and the conformers corresponding to them were named as M1 and M2. Further, new local minima corresponding to the conformers M3, M4 and M5 were revealed in the relaxed scan of C4-C9-C12-N15 dihedral angle. Among the conformers identified till now, M1 was found to be the most stable one and when the relaxed scan was repeated on C1-C6-O18-C21 dihedral angle by taking M1 as the initial geometry, the potential energy surfaces did not reveal any new minima (shown in figure 2.11).

Contrarily, on repeating the relaxed scan on the C4-C9-C12-N15 dihedral angle with M1 as the starting geometry, a new minimum was observed and the corresponding conformer was named as M6 along with the previously identified M1 and M2 conformers. Similarly, in the simultaneous relaxed scan of the two dihedral angles (C4-C9-C12-N15 and C6-C1-O19-C25) the M6 conformer was found to be the global minimum. Additionally, other relaxed dihedral angles were scanned taking M1 conformer as starting geometry, which results in only M1 and M2 conformers. These are shown in the figure 2.11. Thus by exploring conformational landscape of mescaline we observed six conformers and the order of these conformers in their increasing energy are as follows: M6<M1<M2<M5<M3<M4. It is noteworthy to mention that although M1 was only 0.5 kcal/mol higher in energy compared to M6 at the B3LYP/cc-pVTZ level of theory, the two conformers have significantly different structures.

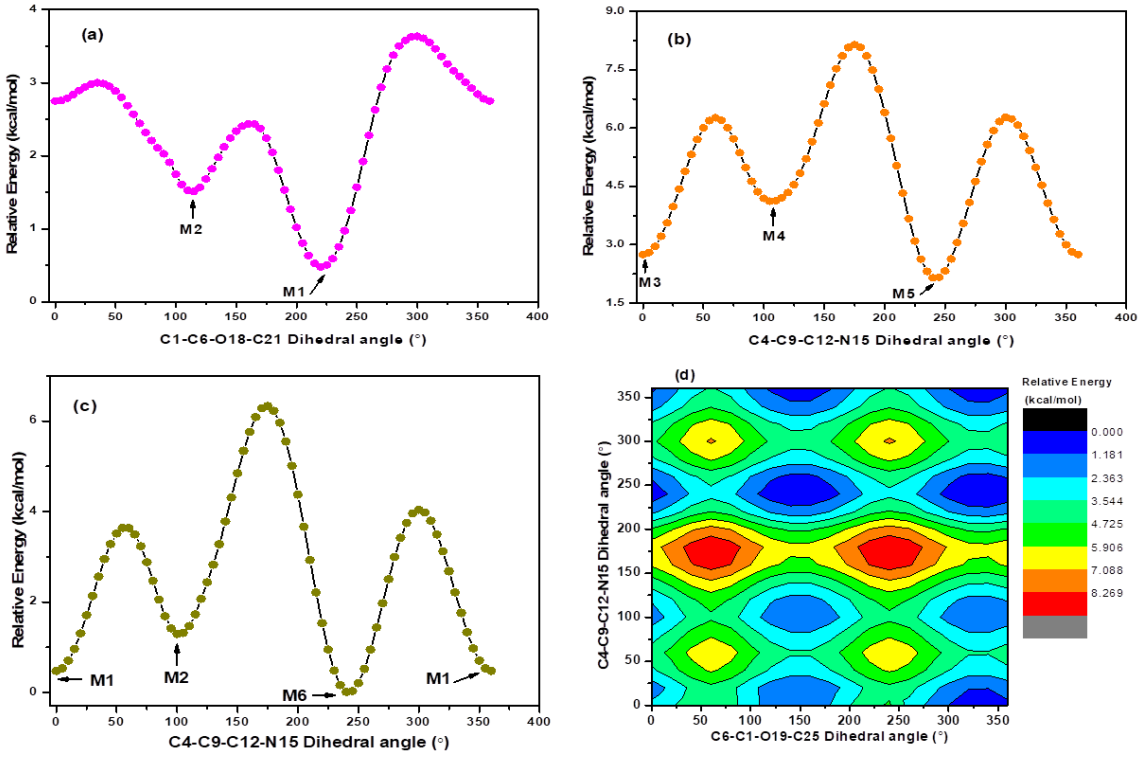

Figure 2.10: (a, b and c) Potential energy curve [with respect to M6-conformer] of mescaline from scanning different dihedral angles and (d) potential energy surface by simultaneous rotation of C1-O19 and C9-C12 bond of mescaline generated at B3LYP/cc-pVTZ level of theory. (Number after the atomic symbol represents the labeling scheme as per Figure 2.12).

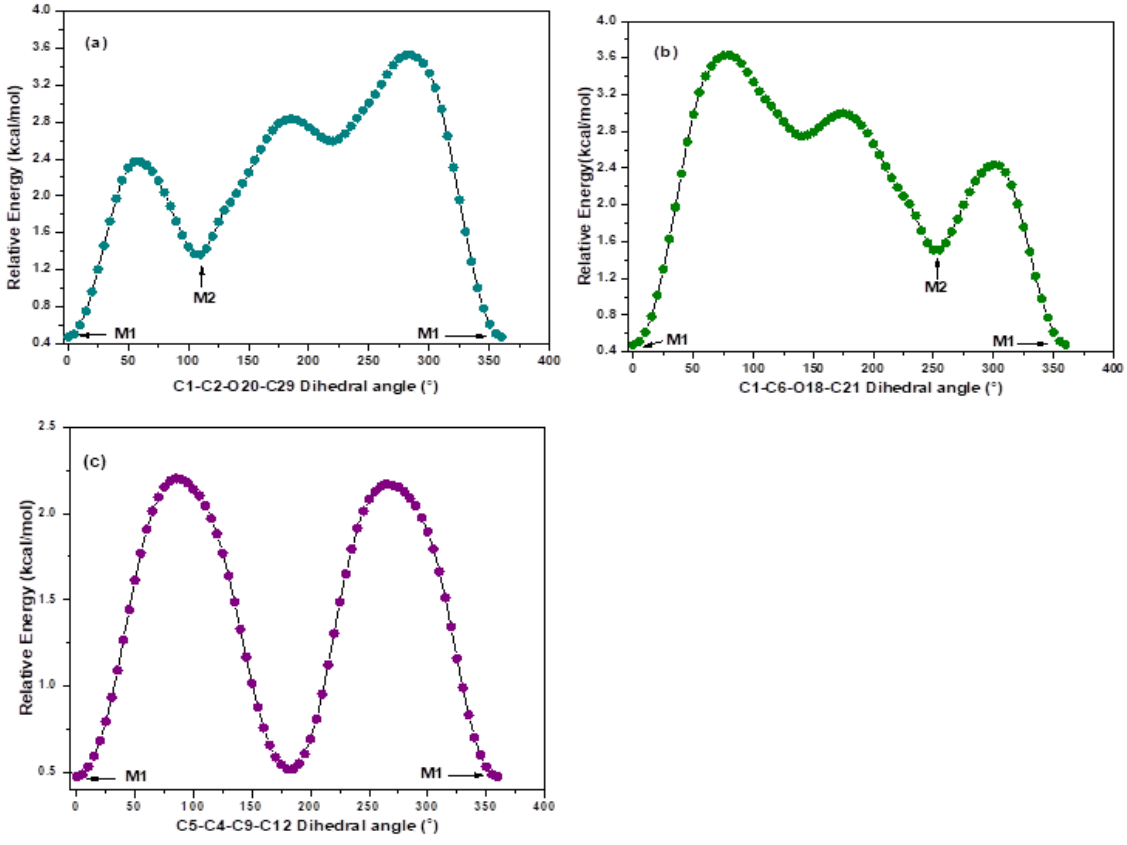

Figure 2.11: (a, b and c) Potential energy curve [with respect to M6-conformer] of mescaline from scanning different dihedral angles B3LYP/cc-pVTZ level of theory. (Number after the atomic symbol represents the labeling scheme as per Figure 2.12).

Consequently, through the use of the Boltzmann distribution equation, the populations of M6 and M1 have been calculated and the results are summarized in table 2.2. From table 2.2, it is evident that while altering the C9-C12 bond to explore the full conformational space, conformer M6 had the highest population, followed by M1. Thus for detailed analysis of mescaline these two conformers M6 and M1 were taken up in the present study.

Table 2.2: Conformational abundance of the mescaline at B3LYP/cc-pVTZ level of theory

Dihedral angle (°)	C4-C9-C12-N15	
	ΔE (kcal/mol)	N_f (%)
0	0.46	**15.27 (Conformer-M1)**
20	1.29	3.77
40	2.94	0.23
60	3.62	0.07
80	2.45	0.53
100	1.28	3.85
120	2.06	1.03
140	3.76	0.06
160	5.75	0.00
180	6.21	0.00
200	4.36	0.02
220	1.52	2.57
240	0	**33.46 (Conformer-M6)**
260	0.93	6.89
280	2.98	0.22
300	4.02	0.04
320	3.11	0.17
340	1.32	3.61
360	0.46	**15.27**

Where, ΔE represents relative energy of a conformer with respect to global minimum structure; N_f is population of different conformers, calculated utilizing Boltzmann distribution equation which is given as equation (1).

2.3.2a Geometrical analysis of psilocybin

Geometrical parameters of both the conformers of psilocybin were computed and compared at the B3LYP/cc-pVTZ level of theory. The calculated geometrical results were found in very good agreement with experimentally reported data.[61] The increase in O30-P31 bond length in conformer-A and conformer-B suggests that the lone pair of O30 is more delocalized towards the indole ring. And the increase in O32-H36 bond length in both the conformers than the O33-H35 bond length suggests the possibility of hydrogen bond formation contributing to the stability of both the conformers. Comparison of the calculated geometrical parameters with experimental data is shown in table 2.3.

Table 2.3: Optimized geometrical parameters of both conformers A & B at B3LYP/cc-pVTZ level of theory

Bond length [Å]	Conformer-A	Conformer-B	Experimental[61]	Bond angle [°]	Conformer-A	Conformer-B	Experimental[61]
R_{N14-C7}	1.38	1.37	1.36	$\theta_{C26N21C22}$	110.7	110.2	110.3
R_{C7-C8}	1.36	1.36	1.36	$\theta_{C26N21C18}$	113.1	111.0	111.7
R_{C8-C2}	1.44	1.44	1.43	$\theta_{C22N21C18}$	110.3	110.3	110.5
R_{C2-C1}	1.41	1.41	1.41	$\theta_{N21C18C15}$	113.3	114.9	114.5
R_{C1-C6}	1.39	1.39	1.38	$\theta_{C18C15C8}$	113.1	116.1	110.5
R_{C6-C5}	1.38	1.38	1.36	$\theta_{C15C8C7}$	127.2	123.2	125.7
R_{C5-C4}	1.40	1.40	1.40	$\theta_{C8C7N14}$	110.1	110.6	111.2
R_{C4-C3}	1.38	1.38	1.37	$\theta_{C7N14C1}$	109.3	109.1	108.8
R_{C3-O30}	1.39	1.38	1.39	$\theta_{N14C1C2}$	106.9	107.0	107.2
$R_{O30-P31}$	1.62	1.62	1.61	θ_{C1C2C8}	107.5	107.6	107.2
$R_{P31-033}$	1.57	1.61	1.49	$\theta_{C15C8C2}$	126.5	131.1	128.1
$R_{P31-O34}$	1.47	1.47	1.47	θ_{C7C8C2}	106.0	105.5	105.7
$R_{P31-O32}$	1.60	1.56	1.55	$\theta_{N14C1C6}$	130.3	130.0	129.7
$R_{O33-H35}$	0.96	0.96	0.89	θ_{C1C6C5}	117.4	117.4	117.5
$R_{O32-H36}$	1.02	1.02	-	θ_{C6C5C4}	121.4	121.4	121.7
R_{C8-C15}	1.49	1.50	1.50	θ_{C5C4C3}	120.4	120.1	120.2
$R_{C15-C18}$	1.53	1.55	1.49	θ_{C4C3C2}	120.3	120.8	120.3
$R_{C18-N21}$	1.47	1.47	1.48	θ_{C3C2C1}	117.6	117.2	117.2
$R_{N21-C26}$	1.46	1.46	1.48	θ_{C2C1C6}	122.7	122.8	123.2
$R_{N21-C22}$	1.46	1.46	1.48	$\theta_{C4C3O30}$	119.7	121.4	123.7
R_{C22-H}	1.08	1.08	0.95	$\theta_{C2C3O30}$	119.6	117.6	116.0
	1.08	1.08	1.10	$\theta_{C3O30P31}$	125.4	124.6	124.5
	1.09	1.09	0.93	$\theta_{O30P31O33}$	104.2	102.8	109.0
R_{C26-H}	1.08	1.08	0.96	$\theta_{O30P31O32}$	100.7	98.6	100.7
	1.08	1.08	1.65	$\theta_{O32P31O34}$	119.6	118.3	117.1
	1.09	1.09	1.00	$\theta_{O34P31O33}$	113.5	112.7	111.3
R_{C18-H}	1.08	1.09	1.12	θ_{C8C2C3}	134.8	135.1	135.6
	1.00	1.08	0.93				
R_{C15-H}	1.09	1.09	0.93				
	1.09	1.09	0.97				
R_{C7-H}	1.07	1.07	0.85				
R_{N14-H}	1.00	1.00	0.87				
R_{C6-H}	1.08	1.08	0.95				
R_{C5-H}	1.08	1.08	0.93				
R_{C4-H}	1.08	1.08	0.99				
R_{C3-C2}	1.40	1.40	1.40				
R_{N14-C1}	1.37	1.37	1.37				

Here, numbers after atoms represent the label of that particular atom in optimized geometry of psilocybin (Figure 2.2).

2.3.2b Geometrical analysis of psilocin

Geometrical parameters of both conformers of psilocin were computed and compared at the B3LYP/cc-pVTZ level of theory. And the obtained geometrical results were found in good agreement with experimentally observed data.[58] The increase in O30-H31 and C18-N21 bond length in conformer-A than conformer-B suggests the possibility of H-bonding between the lone pair of N21 and H31 of O30-H31 bond. Due to which the bond angle of ∠C3O30H31 is increased in conformer-A. These observations are absent in conformer-B. Whereas, in conformer-B, the increase in ∠C4C3O30 and decrease in ∠C2C3O30 suggest the possibility of O30 lone pair interaction with the nearest H atom of C-H bond by analyzing the geometry of this conformer but possibility of such interaction does not seem to be possible in conformer-A. Comparison of the calculated geometrical parameters with experimental data is shown in table 2.4. The population analysis revealed that the conformer-A is the highly dominant conformer for this molecule at ambient conditions.

Table 2.4: Optimized geometrical parameters of conformers A and B at B3LYP/cc-pVTZ level of theory

Bond length [Å]	**A**	**B**	**Experimental Bond length**[58]	**Bond angle [°]**	**A**	**B**	**Experimental Bond angle**[58]
R_{N14-C7}	1.37	1.38	1.38	$\theta_{C23N21C18}$	110.4	114.7	112
R_{C7-C8}	1.36	1.36	1.36	$\theta_{C23N21C22}$	108.9	112.7	109
R_{C8-C2}	1.45	1.44	1.44	$\theta_{C22N21C18}$	112.1	114.7	110
R_{C2-C1}	1.42	1.41	1.41	$\theta_{N21C18C15}$	113.6	117.0	113
R_{C1-C6}	1.39	1.39	1.39	$\theta_{C18C15C8}$	115.5	112.5	113
R_{C6-C5}	1.38	1.38	1.35	$\theta_{C15C8C7}$	122.5	125.8	128
R_{C5-C4}	1.39	1.40	1.41	$\theta_{C8C7N14}$	110.3	110.2	110
R_{C4-C3}	1.38	1.38	1.39	$\theta_{C7N14C1}$	109.3	109.3	109
R_{C3-O30}	1.35	1.37	1.38	$\theta_{N14C1C2}$	107.3	106.8	108
$R_{O30-H31}$	0.99	0.96	-	θ_{C1C2C8}	106.8	107.7	107
R_{C3-C2}	1.41	1.40	1.40	$\theta_{C15C8C2}$	131.3	128.3	126
R_{N14-C1}	1.37	1.37	1.37	θ_{C7C8C2}	106.1	105.7	106

R_{C8-C15}	1.50	1.49	1.50	$\theta_{N14C1C6}$	128.9	129.9	129
$R_{C15-C18}$	1.54	1.54	1.49	θ_{C1C6C5}	116.7	117.0	117
$R_{C18-N21}$	1.47	1.45	1.48	θ_{C6C5C4}	121.3	121.4	122
$R_{N21-C23}$	1.46	1.45	1.48	θ_{C5C4C3}	121.7	120.9	120
$R_{N21-C22}$	1.46	1.44	1.48	θ_{C4C3C2}	118.7	119.6	119
R_{C22-H}	1.08	1.09	1.06	θ_{C3C2C1}	117.5	117.7	119
	1.10	1.10	1.09	θ_{C2C1C6}	123.7	123.1	123
	1.08	1.09	1.07	$\theta_{C4C3O30}$	117.7	122.4	122
R_{C23-H}	1.08	1.09	0.94	$\theta_{C2C3O30}$	123.5	117.9	119
	1.08	1.09	0.97	θ_{C8C2C3}	135.5	134.5	135
	1.10	1.10	1.04	$\theta_{C3O30H31}$	112.2	108.9	-
R_{C18-H}	1.10	1.09	1.04				
	1.09	1.09	0.91				
R_{C15-H}	1.09	1.09	1.02				
	1.09	1.09	1.01				
R_{C7-H}	1.07	1.07	0.95				
R_{N14-H}	1.00	1.00	0.93				
R_{C6-H}	1.08	1.08	1.40				
R_{C5-H}	1.08	1.08	0.98				
R_{C4-H}	1.08	1.08	0.99				

[Note]: numbers after atoms represent the label of that particular atom in optimized geometry of psilocin (Figure 2.7)

2.3.2c Geometrical analysis of mescaline

M6 and M1 conformers underwent another round of geometry optimization at CCSD/cc-pVDZ theoretical level, and the optimized geometries are shown in figure 2.12. At this theoretical level, the energy gap between M6 and M1 was observed to be 1.5 kcal/mol. At this level of theory, the geometrical parameters of both conformers were calculated and then compared, given in table 2.5. The computed geometrical outcomes demonstrated a strong concurrence with the data reported from experimental studies.[59]

The structure of M6 agreed well with the conformer reported by Ernst et al. where the amino group is inclined towards the benzene π cloud. Interestingly, the structure of M1 agreed well with the conformer reported by Tsoucaris et al.[60] where the amino group faces away from the benzene π cloud (staggered form). As the difference between these two conformers was found very less, the conformer M1 (staggered) can also be considered energetically equally favourable. Something similar was predicted by Horn et

al.[62] when they found very small energy difference between the various minima of side chain in case of DOET (2,5-dimethoxy-4-ethyl-α-methyl-phenylethylamine).

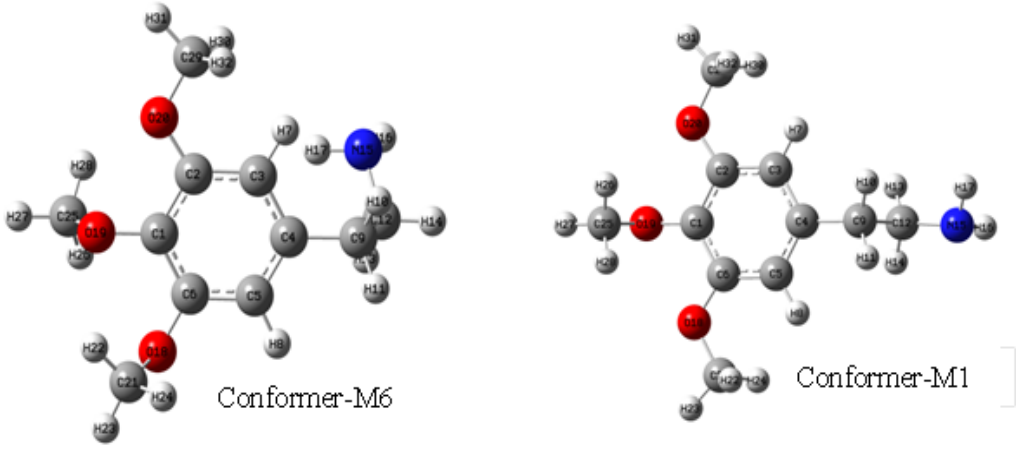

Figure 2.12: Optimized structures of mescaline conformers (M6 and M1) [numbers on atoms represent the label of that atom in the optimized geometry]

Table 2.5: Optimized geometrical parameters of both conformers M6 & M1 at CCSD/cc-pVDZ level of theory

Bond length [Å]	M6	M1	Experimental	Bond angle [°]	M6	M1	Experimental[59]
R_{C4-C3}	1.413	1.406	1.385	θ_{C3C4C5}	119.37	120	120.8
R_{C3-C2}	1.405	1.408	1.353	θ_{C4C3C2}	120.44	120.01	120.6
R_{C2-C1}	1.416	1.409	1.45	θ_{C3C2C1}	119.88	120.14	120.4
R_{C1-C6}	1.403	1.41	1.362	θ_{C2C1C6}	119.45	119.63	118
R_{C6-C5}	1.407	1.408	1.408	θ_{C1C6C5}	120.5	120.14	122.1
R_{C5-C4}	1.402	1.407	1.407	θ_{C6C5C4}	120.31	120.01	117.9
R_{C4-C9}	1.519	1.518	1.512	θ_{C3C4C9}	119.89	120.19	121.4
R_{C9-C12}	1.539	1.537	1.566	θ_{C5C4C9}	120.7	119.75	117.7
$R_{C12-N15}$	1.471	1.471	1.493	$\theta_{C4C9C12}$	112.6	112.18	113.2
R_{C2-O20}	1.366	1.367	1.376	$\theta_{C9C12N15}$	110.42	109.92	110.2
R_{C1-O19}	1.376	1.376	1.358	$\theta_{C3C2O20}$	125.16	124.97	126.1

R_{C6-O18}	1.379	1.367	1.366	$\theta_{C2O20C29}$	116.49	116.69	115.7
$R_{O20-C29}$	1.42	1.419	1.442	$\theta_{O20C2C1}$	114.94	114.87	113.4
$R_{O19-C25}$	1.428	1.426	1.456	$\theta_{C2C1O19}$	119.97	120.17	118.5
$R_{O18-C21}$	1.431	1.419	1.447	$\theta_{C1O19C25}$	111.88	112.11	112.1
				$\theta_{O19C1C6}$	120.56	120.18	123.3
				$\theta_{C1C6O18}$	120.38	114.86	114.2
				$\theta_{C6O18C21}$	113.15	116.67	116.7
				$\theta_{O18C6C5}$	119.08	124.98	123.7

[Note]: numbers after atoms represent the label of that particular atom in optimized geometry of mescaline (Figure 2.12)

2.3.3a FMO of psilocybin

FMO calculation has been very effective in understanding the stability and chemical reactivity of a given molecule. FM orbitals also help understanding the UV spectra, chemical reaction as well as electric and optical properties. The difference between HOMO and LUMO for a particular neutral system is the simplest way to calculate the excitation energy. Here, for the calculation of excitation value (HOMO-LUMO gap), ground state properties of psilocybin was used. HOMO is considered electron donor while LUMO is considered as electron acceptor. For both the conformers FMO calculation was performed at B3LYP/cc-pVTZ level of theory.

It was observed that in both conformers A and B the HOMO is located over the carbon and nitrogen atoms of indole ring and C15, O30 atoms and LUMO is located over C, N atoms of indole and on O30 atom. The difference in the HOMO-LUMO gap of both the conformers was found to be highly insignificant. In both the conformers the calculated HOMO-LUMO gap corresponds to about 240-242 nm, the UV region of the electromagnetic spectrum wherein the $n\rightarrow\pi^*$ and $\pi\rightarrow\pi^*$ electronic transitions occur in both the conformers. And these transitions are responsible for the stability of this molecule. The frontier molecular orbitals are shown in figure 2.13 and all the calculated energy parameters of FMOs for both the conformers of psilocybin are shown in table 2.6.

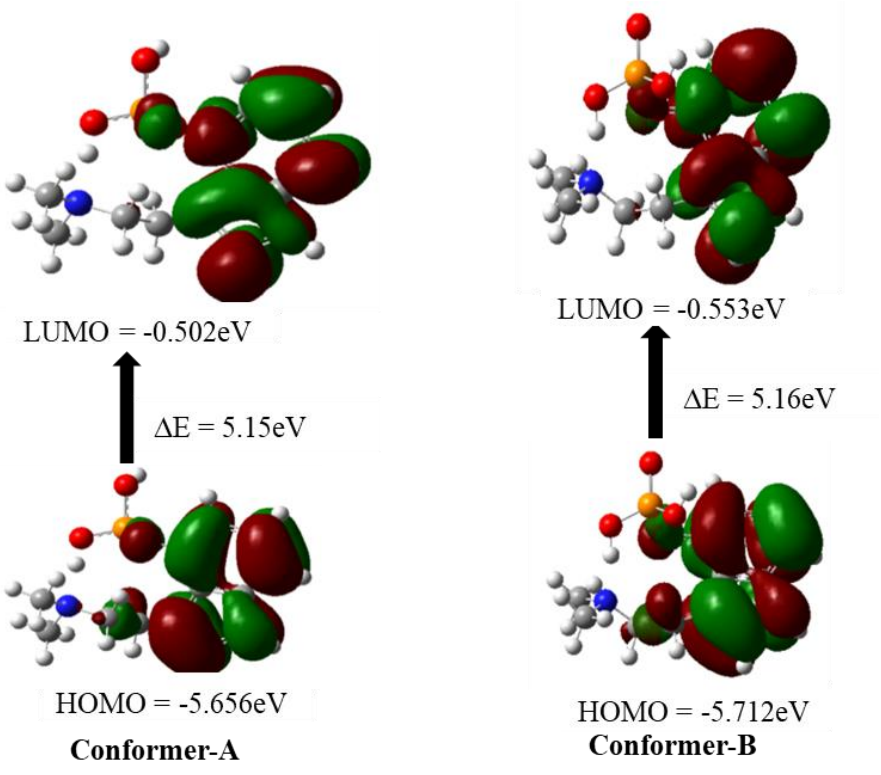

Figure 2.13: HOMO-LUMO (ΔE) gap of both the conformers (A & B) of psilocybin

Table 2.6: Computed energy [eV] parameters of both the conformers (A & B) of Psilocybin at B3LYP/cc-PVTZ level of theory

Energy Parameters	**Conformer-A**	**Conformer-B**
E_{HOMO} (IP) [eV]	-5.66	-5.71
E_{LUMO} (EA) [eV]	-0.50	-0.55
HOMO-LUMO gap [eV]	5.15	5.16
Dipole moment [D]	4.59	7.23
Hardness (η) [eV]	-3.08	-3.13
Chemical potential (μ) [eV]	-2.58	-2.58
Electronegativity (χ) [eV]	-3.08	-3.13
Electrophilicity index (ω) [eV]	-1.08	-1.06

2.3.3b FMO of psilocin

For the calculation of HOMO-LUMO gap, ground state properties of psilocin were used. For both conformers A and B the FMO calculation was performed at B3LYP/cc-pVTZ level of theory. The results of FMO analysis are shown in figure 2.14 and table 2.7. It was observed from the FMO analysis that the HOMO-LUMO gap for conformer-A is slightly more than conformer-B explaining the reason for conformer-B being relatively more reactive than the thermodynamically stable conformer-A. In both these conformers the HOMO-LUMO gap corresponds to about 249-252 nm, the UV region of the electromagnetic spectrum well corroborated by the NBO calculation. And these transitions are responsible for the overall stability of this molecule.

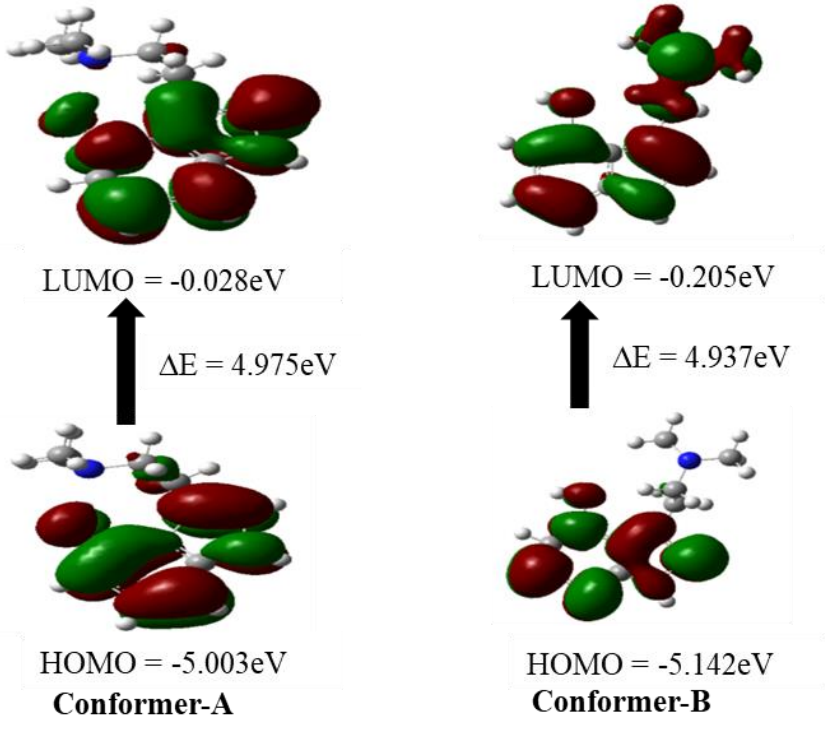

Figure 2.14: HOMO-LUMO (ΔE) gap of both the conformers (A & B) of psilocin molecule

Table 2.7: Computed energy [eV] parameters of conformers (A & B) of Psilocin molecule at B3LYP/cc-PVTZ level of theory

Energy Parameters	**Conformer-A**	**Conformer-B**
E_{HOMO} (IP) [eV]	-5.003	-5.142
E_{LUMO} (EA) [eV]	-0.028	-0.205
HOMO-LUMO gap [eV]	4.975	4.937
Dipole moment [D]	3.990	1.527
Hardness(η) [eV]	-2.515	-2.673
Chemical potential(μ) [eV]	-2.487	-2.468
Electronegativity(χ) [eV]	-2.515	-2.673
Electrophilicity index(ω) [eV]	-1.229	-1.139

2.3.3c FMO of mescaline

To have insight into stability and reactivity of mescaline the FMOs were calculated. The ground state properties of Mescaline were used to calculate the HOMO-LUMO gap. For both the conformers FMO calculation was performed at B3LYP/cc-pVTZ//CCSD/cc-pVDZ level of theory. The difference in the HOMO-LUMO gap of both the conformers was found to be highly insignificant. The HOMO-LUMO gap in these two conformers, which falls within the UV region of the electromagnetic spectrum and corresponds to the $n\rightarrow\pi^*$ and $\pi\rightarrow\pi^*$ electronic transitions in both conformers, is approximately 213-214 nm in wavelength. These transitions play a pivotal role in conferring stability to this molecule. The frontier molecular orbitals are shown in figure 2.15 and all the calculated energy parameters of FMOs for both the conformers of mescaline are given in table 2.8.

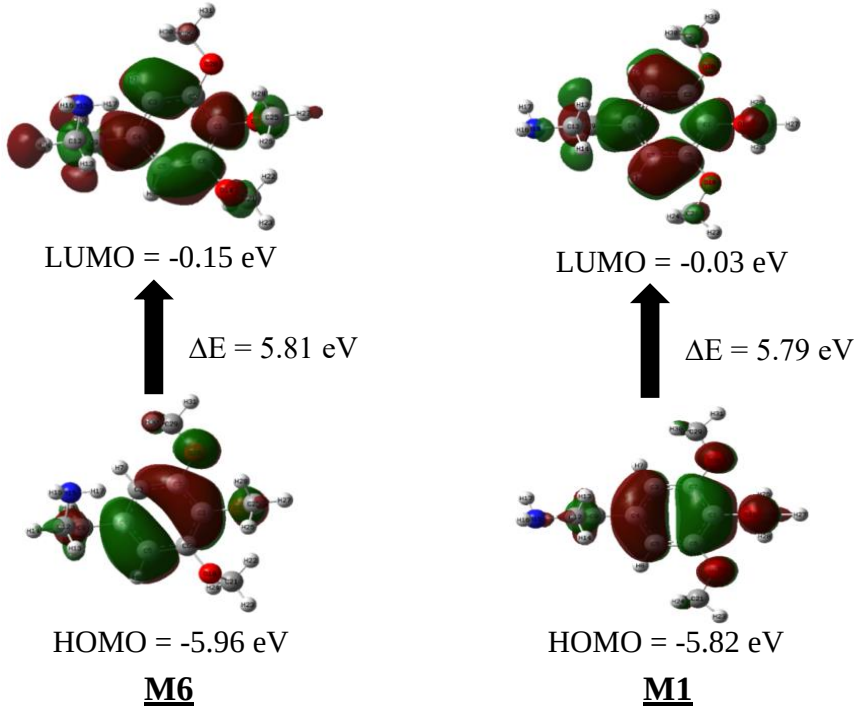

Figure 2.15: HOMO-LUMO (ΔE) gap of both the conformers (M6 & M1) of mescaline

Table 2.8: Computed energy [eV] parameters of both the conformers of mescaline at B3LYP/cc-PVTZ//CCSD/cc-pVDZ level of theory

Energy Parameters	**Conformer-M6**	**Conformer-M1**
E_{HOMO} (IP) [eV]	-5.96	-5.82
E_{LUMO} (EA) [eV]	-0.15	-0.03
HOMO-LUMO gap [eV]	5.81	5.79
Dipole moment [D]	1.22	1.84
Hardness(η) [eV]	-3.05	-2.92
Chemical potential(μ) [eV]	-2.90	-2.89
Electronegativity(χ) [eV]	-3.05	-2.92
Electrophilicity index(ω) [eV]	-1.37	-1.43

2.3.4a NBO of psilocybin

The possibility of different electronic transitions and the exact orbitals involved in electronic transitions besides the types of intramolecular interactions and the extent of charge transfer that may exist in molecule can be analysed with the help of NBO (natural bond orbital) calculation. The charge transfer phenomena can be understood in terms of the second order perturbation energy E(2) resulting from the interaction between the filled orbitals of one system and vacant orbital of another subsystem. The greater the E(2) value the more will be the interaction between each orbital and *vice versa*. The E(2) is calculated by the equation as given in introduction section 1.6.3. From NBO analysis it was observed that in both the conformers A & B the π electrons of indole ring and the lone pair of oxygen in phosphate moiety was extensively delocalized. In both the conformers of psilocybin, while considering the electron pair contributions it was observed that the N21 electron pair was donated to the antibonding orbital σ*(O32-H36) with very high E(2) stabilization energy, i.e. 28.59 kcal/mol in conformer-A while 34.81 kcal/mol in conformer-B, suggesting the H-bond formation between atoms N21 and H36 of O32-H36 bond. Furthermore, hyperconjugative interactions between N21 lone pair and adjacent C-H bonds like n→σ*(C18-H19), n→σ*(C18-H20), n→σ*(C22-H23) and n→σ*(C26-H28) exist.

Also, due to this H-bond formation, the charge density on O32 was comparatively higher indicating an enhanced contribution (with high E(2)) to the antibonding orbital of P-O bond.

Through NBO analysis it was inferred that in both the conformers the formation of strong H-bond between N21 and H36-O32 (H atom of H36-O32 bond) was contributing to the stability. Other orbital interactions in both the conformers were found to be similar. The significant donor-acceptor interactions observed in NBO analysis are shown in table 2.9.

Table 2.9: Some significant donor - acceptor NBO interactions in psilocybin with calculated second order stabilization energies E(2) kcal/mol

Donor	**Acceptor**	**E(2) [kcal/mol]**	
		Conformer-A	**Conformer-B**
πC1-C2	π*C3-O30	5.64	5.32
	σ*C6-H11	2.80	2.75
	π*C8-C15	5.52	5.97
	σ*H12-N14	4.43	4.46
σC1-N14	π*C7-C8	19.55	20.04
πC1-C6	σ*C5-H10	2.70	2.69
πC2-C3	σ*C4-H9	2.25	2.16
πC2-C8	π*C1-C6	4.20	4.08
	π*C3-C4	2.05	2.11
	σ*C7-H13	5.08	5.01
πC3-C4	π*C2-C8	4.48	4.48
	σ*C5-H10	2.24	2.27
	π*C5-C6	19.97	20.10
πC4-C5	σ*C6-H11	2.92	2.95
σC4-H9	π*C2-C3	5.65	5.75
	π*C5-C6	4.32	4.32
πC5-C6	σ*C1-N14	32.94	33.21
	π*C3-C4	16.34	16.18
σC5-H10	π*C1-C6	4.65	4.69
	π*C3-C4	4.52	4.53
σC6-H11	π*C1-C2	4.81	4.85
	π*C4-C5	4.25	4.23
πC7-C8	π*C2-C3	6.08	6.27
	σ*H12-N14	3.37	3.44
	σ*C15-C18	3.46	3.64
σC7-N14	π*C1-C6	4.95	4.98
	π*C7-C8	1.00	0.95
σC15-H16	π*C2-C8	5.85	
	π*C7-C8		3.46
LPN21	σ*C18-H19	5.95	
	σ*C18-H20		5.39
	σ*C22-H23	6.24	5.51

	σ*C26-H28	5.96	5.53
	σ*O32-H36	28.59	34.81
LPO30	π*C3-C4	7.39	5.62
	π*P31-P34	4.67	4.01
	σ*P31-O32	3.20	4.50
	π*C2-C3	6.47	5.09
	σ*P31-O33	9.90	7.26
LPO32	σ*P31-O33	3.59	13.73
	σ*O30-P31	2.41	3.70
	π*P31-O34	2.20	2.89
LPO33	π*P31-P34	5.24	4.84
	σ*O30-P31	9.01	9.81
	σ*P31-O32	6.48	5.32
LPO34	σ*O30-P31	23.89	21.90
	σ*P31-O32	11.68	13.75
	σ*P31-O33	23.49	25.55

Here, LP denotes lone pair of electrons, σ denotes sigma bonding orbital, π denotes pi bonding orbital, π* denotes pi antibonding orbital and numbers after atoms represent the label of respective atom (figure 2.2).

2.3.4b NBO of psilocin

The NBOs of psilocin revealed many π→π* and n→π* intramolecular interactions of very high strength (high E(2) stabilization energy) besides several hyper conjugative interactions in both the conformers. While considering the electron pair contributions in conformer-A, it was observed that the N21 electron pair was donated to antibonding orbital σ*(O30-H31) with very high E(2) stabilization energy, 20.58 kcal/mol suggesting the H-bond formation between N21 and H31 atom of O30-H31 bond. Such kind of H-bond interaction was not observed in conformer-B. But in conformer-B, the hyperconjugative interaction between electron pair of N21 and the nearest σ*(C15-C18) alkyl bond and to the nearest C-H bond i.e. (N21)n→ σ*(C15-C18), (N21)n→ σ*(C22-H26) and (N21)n→ σ*(C23-H28) were observed. These kind of hyperconjugative interactions were obtained with high E(2) stabilization energy in conformer-B than in conformer-A. The significant donor-acceptor interactions inferred from the NBOs are shown in table 2.10.

Table 2.10: Some significant donor - acceptor NBO interactions in psilocin molecule with calculated second order stabilization energies E(2) kcal/mol

Donor	**Acceptor**	**E(2) [kcal/mol]**	
		Conformer-A	**Conformer-B**
π C1-C2	σ*C3-O30	4.78	4.47
	σ*C6-H11	2.73	2.78
	σ*C8-C15	6.09	5.51
	σ*H12-N14	4.40	4.50
	π*C3-C4	22.93	24.92
	π*C5-C6	16.10	16.60
	π*C7-C8	20.59	19.65
π C1-C6	π*C2-C8	1.74	1.74
	σ*C5-H10	2.86	2.83
π C2-C3	σ*C4-H9	2.25	2.52
π C2-C8	π*C1-C6	4.25	4.15
	σ*C7-H13	5.03	5.11
π C3-C4	π*C2-C8	4.72	4.41
	σ*C5-H10	2.33	2.21
	π*C1-C2	14.81	13.62
	π*C5-C6	24.05	21.73
π C4-C5	σ*C3-O30	3.55	4.46
	σ*C6-H11	3.08	2.96
σ C4-H9	π*C2-C3	5.03	4.92
	π*C5-C6	4.39	4.11
π C5-C6	π*C1-C2	21.61	20.24
	π*C3-C4	14.53	14.53
σ C5-H10	π*C1-C6	4.45	4.46
	π*C3-C4	4.57	4.54
σ C6-H11	π*C1-C2	4.89	4.74
π C7-C8	π*C2-C3	5.93	6.09
	σ*H12-N14	3.53	3.41
	π*C1-C2	13.93	15.04
	σ*C15-H17	3.16	2.08
σ C7-H13	π*C2-C8	2.64	2.59
π C7-N14	π* C1-C6	4.76	4.98
σ C15-H16	π*C2-C8	6.58	5.98
σ O30-H31	π*C3-C4	4.10	-
	π*C2-C3	-	5.11

LP N 14	π*C1-C2	36.84	37.50
	π*C7-C8	35.10	32.72
LP N 21	σ*O30-H31	20.58	-
	σ*C15-C18	0.91	10.30
	σ*C22-H26	6.10	9.16
	σ*C23-H28	6.40	9.35
LP O 30	π*C3-C4	25.28	27.40

[Note]: LP denotes lone pair of electrons, σ denotes sigma bonding orbital, π denotes pi bonding orbital, π* denotes pi antibonding orbital and numbers after atoms represent the label of respective atom (figure 2.7)

2.3.4c NBO of mescaline

In case of mescaline, the analysis of NBO calculations unveiled numerous π→π* and n→π* electronic transitions/intramolecular interactions with notably high strength in both conformers (M6 and M1). Additionally, several hyperconjugative interactions were also observed. When examining the electron pair delocalization or charge transfer in both conformers, it was noted that the lone pair of O19 participates in hyperconjugative interactions with the antibonding orbitals π*(C1-C2), π*(C1-C6), and the adjacent σ*(C-H) antibonding orbitals. Analogous hyperconjugative interactions were observed for the other two oxygen atoms, O18 and O20, in both conformers. Similarly, the lone-pair electrons of N15 exhibited very strong hyperconjugative interactions with the σ*(C12-H13) antibonding orbital and a weaker interaction with the σ*(C9-C12) antibonding orbital. Numerous other hyperconjugative interactions were also identified, and their strengths were approximately comparable in both conformers. These interactions play a vital role in providing stability to mescaline. The significant donor-acceptor interactions observed in NBO analysis of mescaline are shown in table 2.11.

Table 2.11: Some significant donor - acceptor NBO interactions in mescaline with calculated second order stabilization energies E(2) kcal/mol at CCSD/cc-pVDZ level

Donor	**Acceptor**	**E(2) [kcal/mol]**	
		M7	**M1**
πC1-C2	σ*C3-H7	3.17	3.20
	σ*C6-O18	4.43	3.41
	σ *O20-C29	3.94	3.97
	π*C1-C6	4.53	4.31
	π*C2-C3	4.97	5.01
	σ*O19-C25	1.45	1.77
	π*C3-C4	-	31.02
	π*C5-C6	-	55.75
πC1-C6	π*C1-C2	4.63	4.31
	σ*C2-O20	3.33	3.42
	π*C5-C6	4.63	5.00
	σ*C5-H8	2.69	3.19
	σ*O18-C21	1.08	3.97
	σ*O19-C25	1.55	1.46
	π*C2-C3	47.52	-
	π*C4-C5	31.34	-
	σ*O18-C21	1.09	3.97
	σ*O19-C25	1.61	1.46
σ C1-O19	π*C2-C3	2.15	2.27
	π*C5-C6	2.22	2.26
	π*C1-C2	0.94	1.04
	π*C1-C6	1.04	1.04
	σ*C25-H27	1.51	1.54
πC2-C3	σ*C1-O19	4.17	4.14
	σ*C3-H7	1.77	1.73
	σ*C4-C9	3.84	4.08
	π*C1-C6	30.08	
	π*C4-C5	48.57	
	π*C1-C2	5.37	5.37
	π*C3-C4	4.51	4.54
σ C2-O20	π*C1-C6	2.41	2.56
	π*C3-C4	1.63	1.58
πC3-C4	π*C2-C3	4.55	4.56
	σ*C2-O20	5.82	5.71
	π*C4-C5	4.57	4.78
	σ*C5-H8	3.40	3.15
	π*C1-C2	-	50.63

	π*C5-C6	-	26.11
	σ*C9-C12	-	3.38
σ C3-H7	π*C1-C2	5.35	5.09
	π*C4-C5	5.49	5.69
πC4-C5	σ*C6-O18	4.72	5.74
	π*C1-C6	48.29	-
	π*C2-C3	29.28	-
	σ*C9-C12	3.53	-
	π*C3 –C4	-	4.78
	σ*C3-H7	-	3.20
	π*C5-C6	-	4.53
πC4-C9	π*C2-C3	3.68	3.60
	σ*C4-C5	3.39	3.33
	π*C5-C6	3.40	3.62
πC5-C6	σ*C1-O19	4.73	4.13
	σ*C4-C9	4.44	4.05
	σ*O18–C21	2.00	-
	π*C1-C6	4.71	5.36
	π*C4-C5	4.17	4.53
	π*C1-C2	-	28.87
	π*C3-C4	-	56.24
σ C5-H8	π*C1-C6	5.57	5.13
	π*C3-C4	5.68	5.71
	π*C4-C5	1.67	1.74
	π*C5-C6	1.04	1.20
σ C6-O18	π*C1-C2	2.37	2.56
σ C9-H10	π*C4-C5	4.63	4.79
σ C9 –H11	π*C3-C4	4.92	4.62
	π*C4-C5	1.11	-
	σ*C12-N15	5.22	-
	σ*C12-H13	-	4.52
σ C9-C12	π*C4-C5	3.64	0.71
	π*C3-C4	-	3.88
	σ*C4-C9	1.37	1.28
	σ*N15-H16	2.84	2.71
σ C12-H13	σ*C9-H10	4.34	-
	σ*C9-H11	-	4.37
σ C12-H14	σ*C4-C9	5.08	-
	σ*N15-H17	4.48	4.62
σ C12-N15	σ*C9-H11	2.19	-
	σ*C4-C9	-	2.75
σ N15-H16	σ*C9-C12	4.82	4.46
σ N15-H17	σ*C12-H14	4.01	4.20

σ O18-C21	π*C1-C6	3.97	3.76
σ O19-C25	π*C1-C6	3.99	1.01
σ O20-C29	π*C1-C2	3.86	3.74
σ C21-H23	σ*C6-O18	4.44	4.96
σ C25-H27	σ*C1-O19	4.34	4.39
σ C29-H31	σ*C2-O20	4.94	4.96
LP N15	σ*C9-C12	1.28	1.13
	σ*C12-H13	10.88	11.10
LP O18	σ*C21-H22	5.13	7.58
	σ*C21-H23	1.82	2.60
	σ*C21-H24	8.60	7.58
	π*C1-C6	9.13	0.71
	π*C5-C6	6.67	36.94
LP O19	σ*C25-H27	2.08	2.14
	π*C1-C2	9.90	9.41
	π*C1-C6	7.83	9.33
	σ*C25-H26	6.33	7.43
	σ*C25-H28	7.88	7.33
LP O20	σ*C29-H32	1.63	7.62
	π*C2-C3	36.89	9.00
	π*C1-C2	0.73	33.83
	σ*C29-H30	7.47	7.62
	σ*C29-H32	7.55	7.62

[Note]: LP denotes lone pair of electrons, σ denotes sigma bonding orbital, π denotes pi bonding orbital, π* denotes pi antibonding orbital and numbers after atoms represent the label of respective atom (figure 2.12)

2.3.5a AIM analysis of psilocybin

AIM calculations are reportedly found very helpful to get insight on the type of molecular interaction through electron density calculation ρ(r) and Laplacian electron density $\nabla^2\rho(r)$ calculation.

In the AIM calculation of conformer-A of psilocybin, 3 intramolecular H-bonds were observed. Among them the H-bonds between N21 and H36 was observed of medium strength and partially covalent. Conformer-B showed only two intramolecular H-bonds between N21 and H36 which is also of medium strength and partially covalent but it is stronger than what was observed in conformer-A. Furthermore, it has a very weak H-bond interaction between O33 and H16. These interaction energies (H-bond energies)

were calculated by equation established by Emamian et al.[63] The approach by Espinosa and colleagues,[64] which estimates H-bond energies as E = V(r)/2, tends to overestimate H-bond energy and thus was not utilized. All these interactions were of significant energies. Thus by the analysis of AIM results it can be suggested that the hydrogen bond between N21 and H36 are the major contributor towards the stability of conformer-A and conformer-B. The AIM results support the NBO results very well. At BCP (3,-1) the calculated parameters of AIM analysis are summarized in table 2.12 and basin surfaces of corresponding BCP are shown in figure 2.16.

Table 2.12: Topological parameters for bonds of interacting atoms in psilocybin: electron density (ρBCP), kinetic electron energy density (GBCP), potential electron energy density (VBCP), total electron energy density (HBCP), Laplacian of electron density (∇^2 BCP), estimated interaction energy (E_{int}) at bond critical point (BCP)

Conformer-A						
Critical Point number	**ρBCP [a.u.]**	**G_{BCP} [a.u.]**	**V_{BCP} [a.u.]**	**H_{BCP} [a.u.]**	**∇^2ρBCP [a.u.]**	**E_{int} [kcal/mol]**
24[O30-H20]	0.0101	0.0076	-0.0059	0.0018	0.0376	-1.51
25[N21-H36]	0.0603	0.0327	-0.0548	-0.0022	0.0424	-12.71
35[O34-H17]	0.0104	0.0069	-0.0056	0.0013	0.0330	-1.58
Conformer-B						
64[N21-H36]	0.0682	0.03721	-0.0650	-0.0278	0.0376	-14.47
67[O33-H16]	0.0032	0.0023	-0.0016	0.0006	0.0117	-0.03

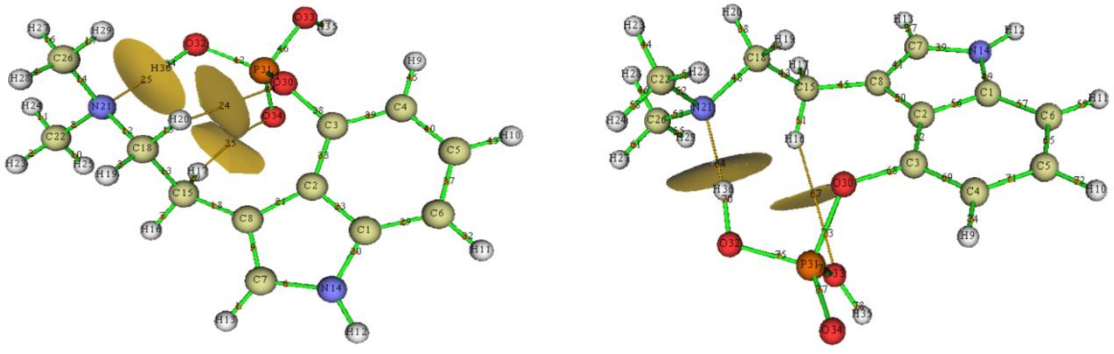

Conformer-A Conformer-B

Figure 2.16: Topological basin surfaces with Bond critical points (3,-1) of psilocybin at B3LYP/cc-pVTZ level for the Conformer-A and Conformer-B of psilocybin

2.3.5b AIM analysis of psilocin

Topological analysis of BCP revealed that there were 3 and 2 kinds of hydrogen bonds in conformer-A and conformer-B, respectively. AIM calculation of conformer-A revealed two intramolecular interactions. One of the H-bond interactions of medium strength and thereby partially covalent was observed between N21 and H31 of O30-H31 bond. Its interaction energy was calculated to be -10.77 kcal/mol. The second interaction was of very weak nature and observed between H17 and H24 atoms. In conformer-B, two weak intramolecular H-bond interactions were observed between O30----H17-C and O30----H20-C moieties in psilocin. These interactions were comparatively very weak. Thus from the analysis of AIM results it is concluded that the hydrogen bond between N21 and H36 is the major contributor towards the stability in conformer-A than conformer-B.

AIM calculations attribute the stability of conformer-A to the intramolecular H-bond formation between the nitrogen of ethylamine and the indolic OH. This reinforces the rationale hypothesized by Cyrus et al.[29] Contrarily in the X-ray crystal structure study of psilocin carried out by T. J. Petcher et al.[58] only one conformer was observed along with categorically precluding the possibility of any intramolecular H-bonding. Therefore, to determine the strength of intramolecular and intermolecular H-bonding in psilocin

molecule its dimers were taken up for further studies. As conformer-A and B were found stable and most populated conformers among all the conformers, only these were used further for dimers calculations.

Different dimers, designated as Conformer-D1, D2, D3, D4, D5 and D6, were explored in order to cover all possible intermolecular H-bonds. These dimers were optimized at B3LYP/cc-pVTZ level of theory and their interaction energies were corrected for the basis set superposition error. The optimized geometry of these dimers are shown in Figure 2.17 and their interaction energies are shown in the table 2.13. Conformer-D1, dimer of conformer-A, has both intramolecular H-bonding between N of ethyl amine and indolic OH as well as intermolecular H-bonding between ring NH of one molecule and indolic OH of other molecule. Similarly, in conformer-D5 and D6 which are dimers of conformer-A having both molecules oriented in parallel position in D5 and T shaped in D6 conformer. While conformers D2, D3 and D4 consist of dimer of conformer-B where there is intermolecular H-bond formation between indolic OH of both molecules in D2 and between OH of one molecule and N of ethyl amine of another molecule in D3 while in D4 it was formed between OH and NH of indole ring. The calculated parameters of AIM analysis at BCP (3,-1) for monomers and all the dimers are also summarized in table 2.14 and the basin surfaces of corresponding BCP are shown in Figure 2.18.

Through AIM analysis of dimers as shown in table 2.10, it was revealed that in case of dimers of conformer-A namely conformers-D1, D5 and D6, intramolecular H-bond interaction was much stronger than intermolecular H-bond interaction while in case of dimers of conformer-B, namely conformers-D2, D3 and D4, intermolecular H-bond interaction was much stronger than intramolecular H-bond interactions. It must be noted that when the dimers were subjected to geometry optimization, the highest interaction energies (shown in table 2.13) were obtained for conformers of D1 and D3 and were also comparable to each other. But in crystal structure of psilocin only one conformer was observed having only intermolecular H-bond interactions, in accordance with the predictions pertaining to conformer-B. It was reported in literature that glycolic acid shows different kind of H-bonding in its crystal structure and in gas phase. In its crystal

structure the intermolecular H-bonding is dominant while in its gas phase only intramolecular H-bonding is dominant.[66] Similarly, present computational study was carried out in gas phase where the psilocin molecule showed strong intramolecular H-bond interaction in the most stable conformer which opposes the prediction made in its crystal structure study.[58] The variation in stabilization pathways between the crystal and gas phases could potentially arise from the reduced repulsion among psilocin molecules. This reduction may be attributed to the development of intermolecular hydrogen bonding between the indolic OH group and the ethylamine nitrogen, resulting in crystal stability. Conversely, in the gas phase, the prevalence of intermolecular hydrogen bonding diminishes, giving way to the predominance of intramolecular hydrogen bonding. Intramolecular H-bond interaction results in the formation of an 8-memebered ring which may be contributing to its stability in the gas phase. This prediction was made earlier by Cyrus et al.[29] which is validated now through this computational study.

Table 2.13: BSSE Corrected Interaction energy of all the dimers of Psilocin at B3LYP/cc-pVTZ level of theory

Dimers of Psilocin molecule	**BSSE corrected Interaction Energy [kcal/mol]**
Conformer-D1	-7.63
Conformer-D2	-3.19
Conformer-D3	-7.49
Conformer-D4	-2.70
Conformer-D5	-2.98
Conformer-D6	-5.67

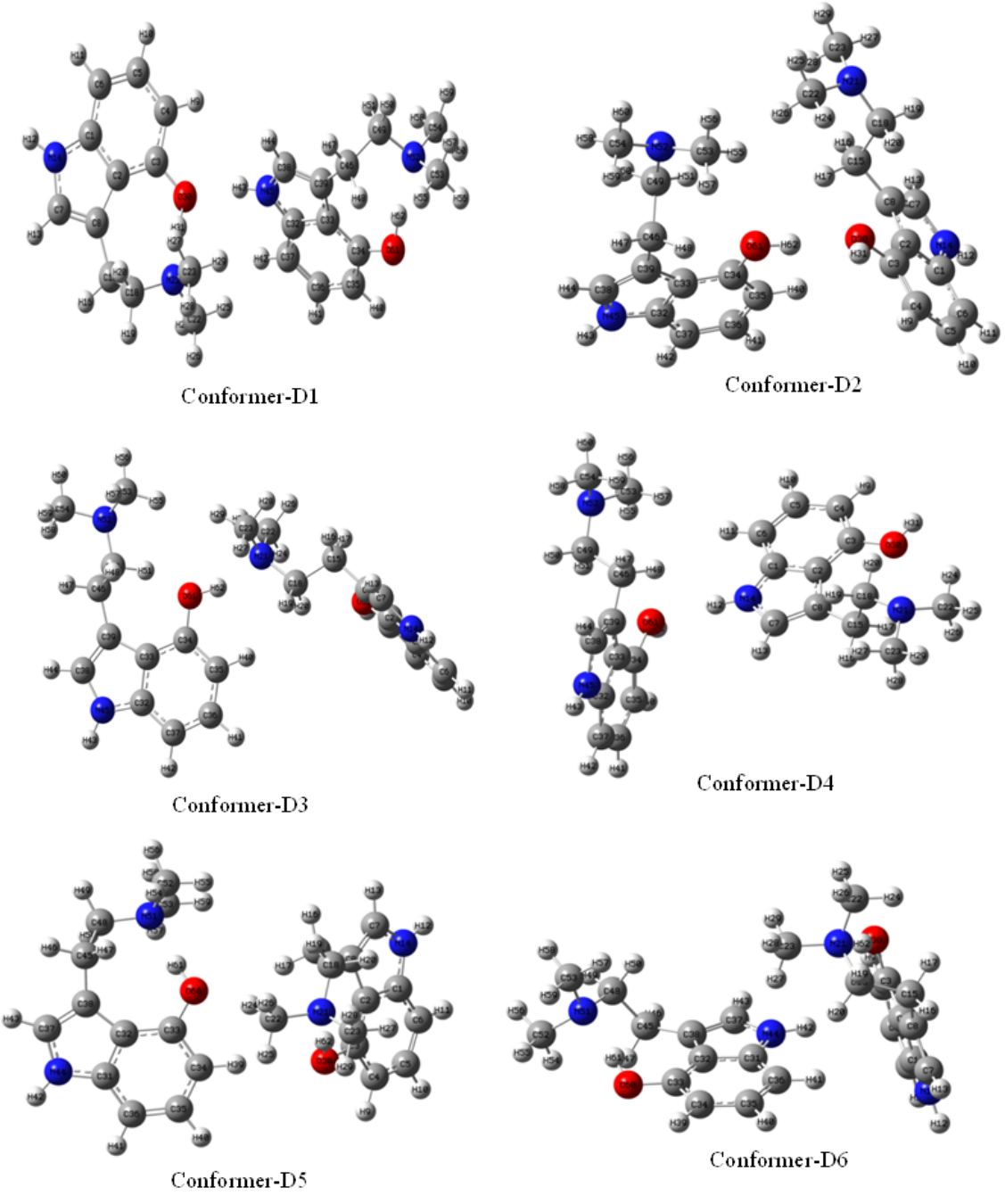

Figure 2.17: Optimized structures of all the dimers of psilocin molecule at B3LYP/cc-pVTZ level of theory

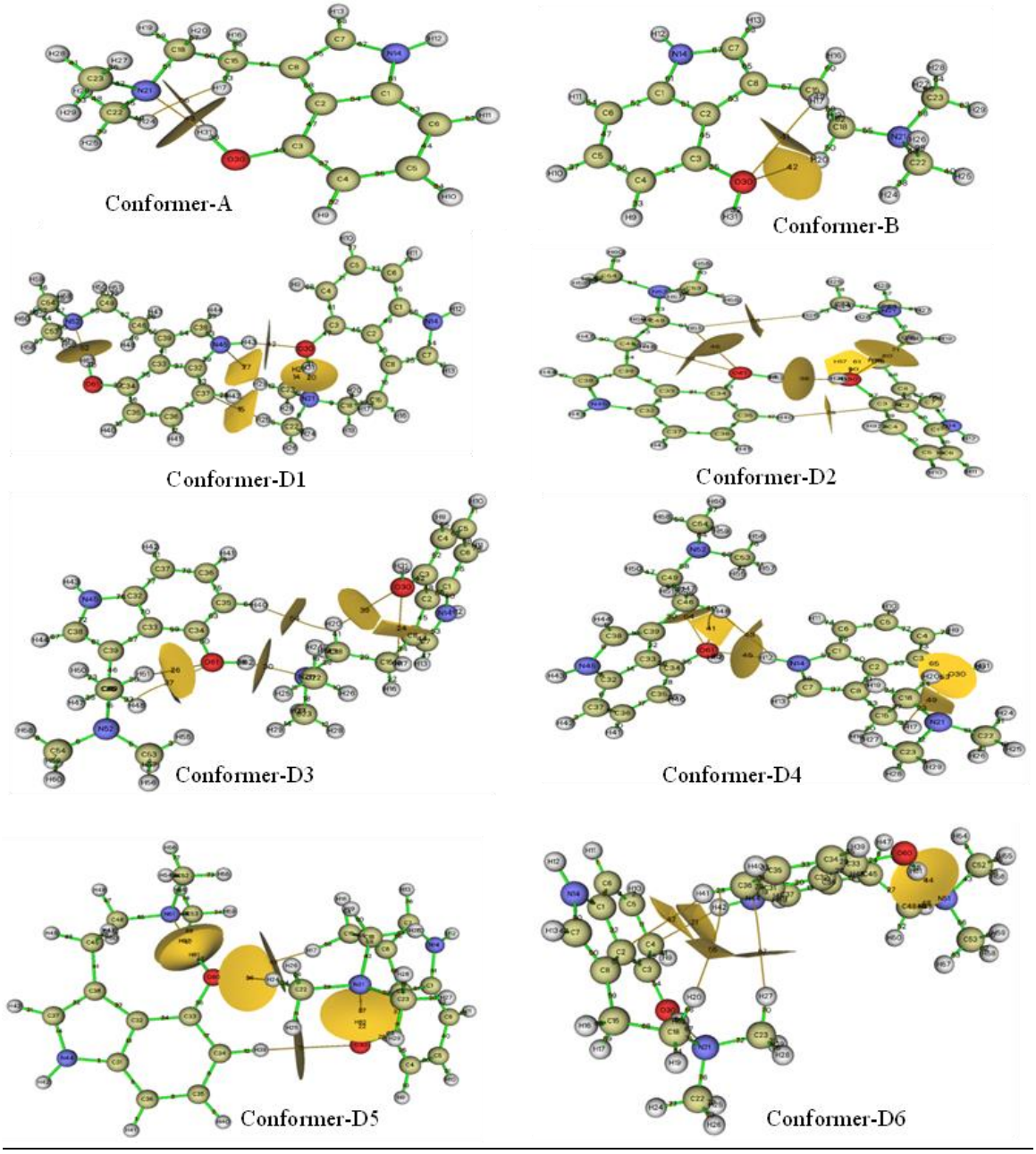

Figure 2.18: Topological basin surface with Bond critical points (3, -1) of psilocin at B3LYP/cc-pVTZ level for Monomers (A and B conformers) and all the dimers of psilocin molecule

Table 2.14: Topological parameters for bonds of interacting atoms in psilocin (for monomers and dimers): electron density (ρBCP), kinetic electron energy density (GBCP), potential electron energy density (VBCP), total electron energy density (HBCP), Laplacian of electron density (∇^2 BCP), estimated interaction energy (E_{int}) at bond critical point (BCP)

Conformer-A						
Critical Point number	**ρBCP [a.u.]**	**G_{BCP} [a.u.]**	**V_{BCP} [a.u.]**	**H_{BCP} [a.u.]**	**∇^2ρBCP [a.u.]**	**E_{int} [kcal/mol]**
43[N21----H31]	0.0516	0.0309	-0.0462	-0.0153	0.0624	-10.77
56[H17----H24]	0.0128	0.0093	-0.0074	0.0018	0.0445	-2.11
Conformer-B						
41[O30----H17]	0.0064	0.0054	-0.0038	0.0015	0.0280	-0.68
42[O30----H20]	0.0062	0.0044	-0.0033	0.0010	0.0218	-0.64
Conformer-D1						
15[C37----H25]	0.00311	0.00176	-0.00118	0.00058	0.00935	-0.05
20[N21----H31O30]	0.06074	0.03460	-0.05639	-0.02179	0.05122	-12.81
27[N45----H29]	0.00207	0.00125	-0.00087	0.00038	0.00653	-0.28
42[O30----H43N45]	0.02470	0.0196	-0.0189	0.00079	0.08193	-4.77
52[N52----H62O61]	0.05161	0.03066	-0.04601	-0.01535	0.06121	-10.77
Conformer-D2						
26[C3----H40]	0.00280	0.00174	-0.00115	0.00059	0.00933	-0.12
33[O61----H48]	0.00653	0.00540	-0.00389	0.00151	0.02763	-0.71
38[O30----H62O61]	0.02366	0.01859	-0.01817	0.00043	0.07610	-4.53
45[O61----H51]	0.00638	0.00459	-0.00349	0.00109	0.02277	-0.68
50[O30----H17]	0.00628	0.00516	-0.00367	0.00149	0.02663	-0.66
60[O30----H20]	0.00510	0.00364	-0.00279	0.00085	0.01803	-0.39
Conformer-D3						
24[O30----H17]	0.00638	0.00539	-0.00381	0.00157	0.02787	-0.68
26[O60----H51]	0.00641	0.00457	-0.00351	0.00106	0.02251	-0.69
30[N21----H62O61]	0.04197	0.02513	-0.03453	-0.00939	0.06298	-8.62
37[O61----H48]	0.00685	0.00560	-0.00407	0.00153	0.02852	-0.78
39[O30----H20]	0.00687	0.00499	-0.00377	0.00121	0.02482	-0.79
54[H40----H20]	0.00482	0.00334	-0.00242	0.00092	0.01705	-0.33
Conformer-D4						
41[O61----H48]	0.00619	0.00513	-0.00364	0.00149	0.02647	-0.64
45[O61----H12N14]	0.01769	0.01376	-0.01203	0.00173	0.06199	-3.20
49[O30----H17]	0.00646	0.00538	-0.00382	0.00156	0.02781	-0.70
53[O30----H20]	0.00610	0.00440	-0.00334	0.00106	0.02185	-0.62
54[O61----H51]	0.00535	0.00381	-0.00293	0.00089	0.01879	-0.45
Conformer-D5						

15[O30----H39]	0.00649	0.00435	-0.00338	0.00097	0.02131	-0.71
27[N21----H62O30]	0.05413	0.03165	-0.04879	-0.01714	0.05806	-11.33
36[O60----H24]	0.00794	0.00566	-0.00429	0.00136	0.02808	-1.03
45[O60----H17]	0.00539	0.00356	-0.00278	0.00078	0.01736	-0.46
57[N51----H61O60]	0.05295	0.03122	-0.04758	-0.01636	0.05942	-11.07
Conformer-D6						
21 [H42----C4]	0.00931	0.00561	-0.00457	0.00104	0.02661	-1.33
42[H41----C2]	0.00336	0.00209	-0.00145	0.00064	0.01094	-0.01
44[N51----H61O60]	0.05201	0.03087	-0.04648	-0.01561	0.06108	-10.86
57[H27----N44]	0.00348	0.00191	-0.00131	0.00059	0.01002	-0.03
67[N21----H62O30]	0.05698	0.03304	-0.05208	-0.01904	0.05600	-11.97

2.3.5c AIM analysis of mescaline

In the AIM calculation of M6, one intramolecular H-bond was observed between O19 and H22 [O19---H22], shown in figure 2.19 which was of weak in nature having -2.02 kcal/mol ineraction energy. In M1 no such interaction was observed. Thus it is surmised that this intramolecular hydrogen bond, although weak, may still contribute to the stability of M6 vis-à-vis M1.

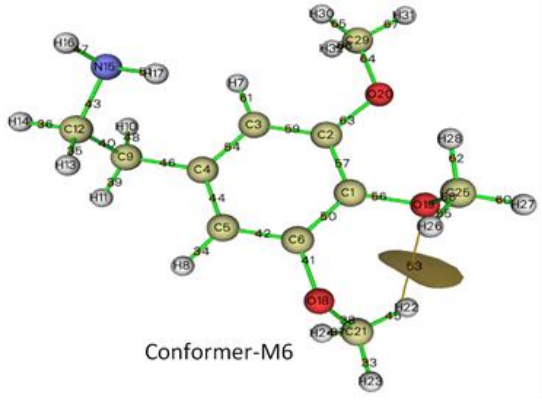

Figure 2.19: Topological basin surfaces with Bond critical points (3,-1) of mescaline at CCSD/cc-pVDZ level for the Conformer-M6 of mescaline

2.3.6 RDG analysis of mescaline

Furthermore, to discriminate and visualise the several types of non-covalent interactions in mescaline, RDG calculation was carried out which is based on electron density and its derivatives published by Jhonson et al. in 2010.[67] To clearly portray different sorts of

interactions, a colour gradient representing ρ(r) and λ2 value was utilized to fill up the RDG isosurfaces, as shown in figure 2.20(b). The contour value has been set to 0.5. Multiwfn and VMD softwares were used to compute and visualize these findings. The interaction zones highlighted in blue in figure 2.20(b) are H-bond interactions, whereas those highlighted in green are Van der Waals interactions and those highlighted in red are repulsive interactions. The scatter plot and RDG isosurface for conformers M6 and M1 are shown in figure 2.20(a) from where the existence of intramolecular H-bond interaction between O---H-C is inferred. Weak Van der Waals interaction was observed between N-H----π of benzene ring in M6 while in M1 weak Van der Waals interactions was observed only in O---H-C. These H-bond interactions contribute to relatively higher stability of M6 than M1.

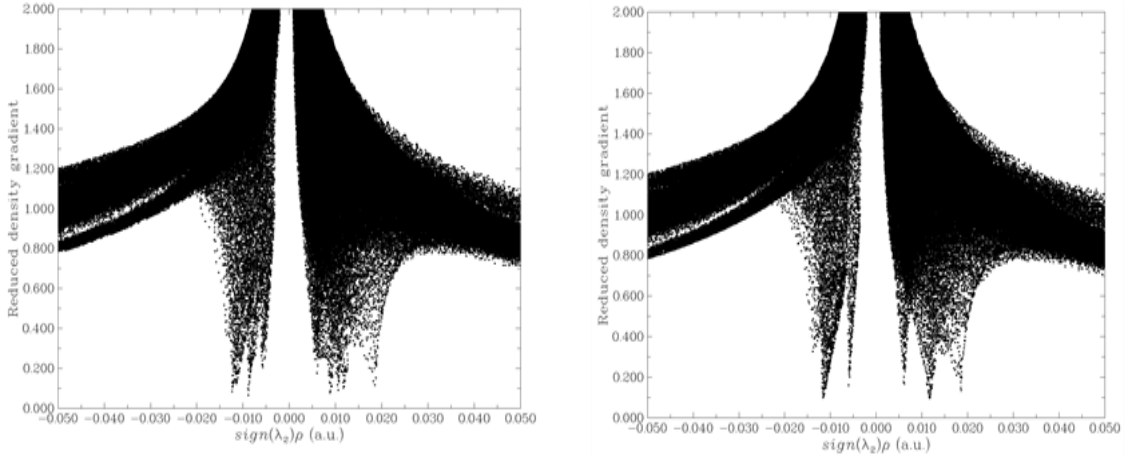

Figure 2.20(a): Scatter plot of the reduced density gradient (RDG(r)) versus Ω(r) for M6 and M1 conformers of mescaline [where, iso-surface of RDG = 0.5]

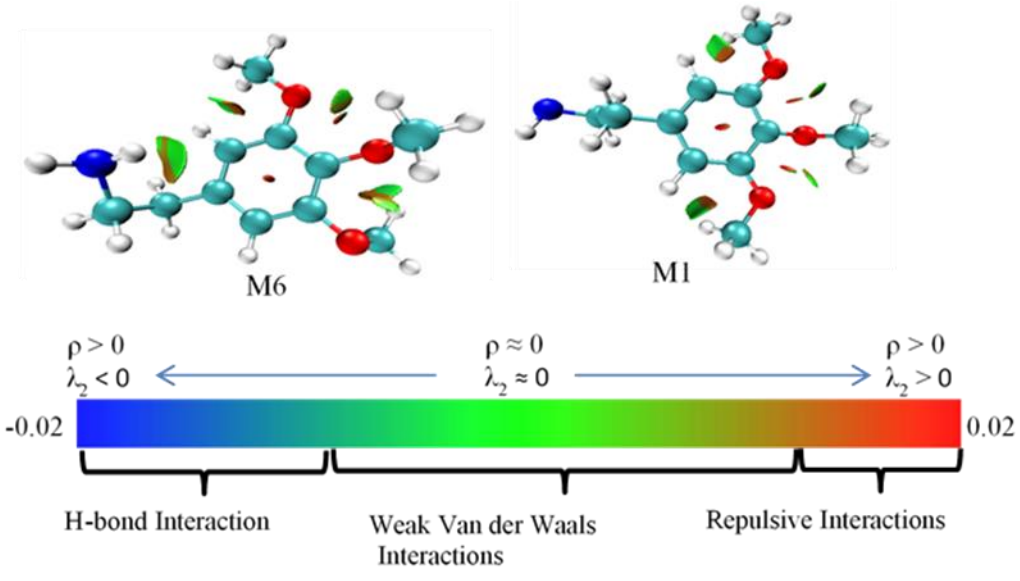

Figure 2.20(b): The visual diagram of RDG iso-surfaces for mescaline conformers (M6 and M1). Color gradient corresponds to the different types of interaction in respective conformers

2.3.7a Charge analysis of psilocybin

To understand how the above mentioned intramolecuar charge transfers affect the charges on each atom, ESP[MK(Merz Kollman)] charge calculation was done at the B3LYP/cc-pVTZ level of theory. Since in literature ESP[MK] charge calculations have been found more reliable and efficient over Mulliken charge population analysis,[68] therefore here ESP[MK] charge calculation was preferred over Mulliken charge calculation. By ESP[MK] charge analysis it was observed that in both the conformers-A and B of psilocybin, there is more negative charge on N14 atom compared to N21 which suggests that the lone pair electron of N21 is donated to adjacent H36 atom and due to which the negative charge on O32 increases and the positive charge on H36 atom decreases. This imparts stability to conformer-A and conformerB. These observations support the above explained AIM and NBO results. Charge distribution plot for ESP[MK] calculation is shown in Figure 2.21. Hirshfeld charge calculation was also performed for both the conformers and very slight differences were observed from ESP[MK] charge calculation.

The charge distribution curve of Hirshfeld charge calculation is shown in figure 2.22 and the charge value on each atom are shown in table 2.15.

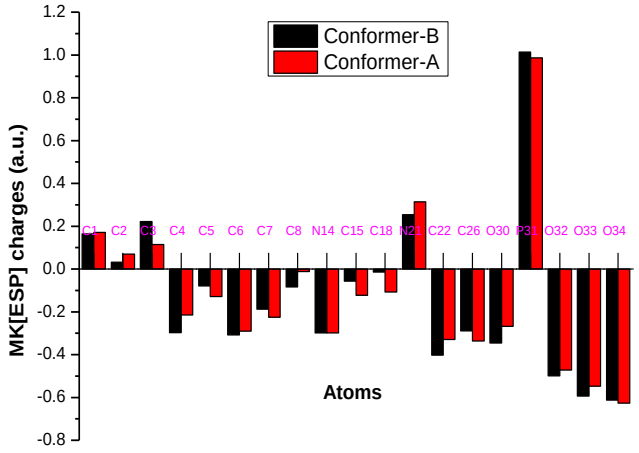

Figure 2.21: Charge distribution plot of ESP[MK] charges for conformer-A and conformer-B ; the number after atoms represent the label of that atom shown in figure 2.2

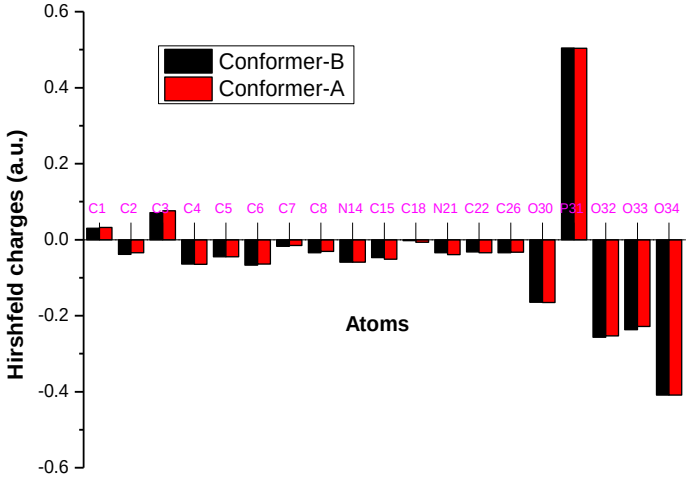

Figure 2.22: Charge distribution plot of Hirshfeld charges for conformer-A and conformer-B

Table 2.15: The Hirshefield and ESP[MK] charge values [a.u.] on each atom of both the conformers (A & B) of psilocybin molecule

No.	Atoms	Charge Values [a.u.]			
		Conformer-A		Conformer-B	
		ESP[MK]	Hirshfeld	ESP[MK]	Hirshfeld
1	C	0.171	0.032	0.163	0.030
2	C	0.070	-0.034	0.032	-0.038
3	C	0.115	0.076	0.222	0.071
4	C	-0.215	-0.065	-0.297	-0.064
5	C	-0.129	-0.045	-0.078	-0.044
6	C	-0.290	-0.064	-0.308	-0.066
7	C	-0.225	-0.015	-0.187	-0.017
8	C	-0.012	-0.031	-0.084	-0.034
9	H	0.141	0.040	0.177	0.045
10	H	0.138	0.038	0.128	0.040
11	H	0.152	0.037	0.155	0.036
12	H	0.323	0.141	0.325	0.141
13	H	0.178	0.048	0.169	0.047
14	N	-0.299	-0.059	-0.298	-0.059
15	C	-0.123	-0.051	-0.056	-0.047
16	H	0.073	0.029	0.058	0.032
17	H	0.085	0.031	0.048	0.030
18	C	-0.107	-0.007	-0.014	-0.002
19	H	0.038	0.019	0.044	0.033
20	H	0.052	0.030	0.017	0.022
21	N	0.314	-0.039	0.253	-0.034
22	C	-0.329	-0.034	-0.401	-0.031
23	H	0.085	0.025	0.093	0.026
24	H	0.105	0.040	0.141	0.043
25	H	0.100	0.042	0.130	0.043
26	C	-0.336	-0.033	-0.289	-0.033
27	H	0.117	0.040	0.112	0.043
28	H	0.072	0.025	0.073	0.025
29	H	0.116	0.043	0.091	0.041
30	O	-0.268	-0.165	-0.345	-0.164
31	P	0.987	0.504	1.014	0.504
32	O	-0.472	-0.253	-0.499	-0.256
33	O	-0.547	-0.228	-0.594	-0.236
34	O	-0.627	-0.409	-0.612	-0.408
35	H	0.405	0.184	0.414	0.181
36	H	0.136	0.109	0.200	0.102

Here, numbers represent label of that atom (figure 2.2).

2.3.7b Charge analysis of psilocin

Similarly, for psilocin, Hirshfeld charge calculation was carried out for its both conformer-A and B at the B3LYP/cc-pVTZ level of theory. And the results of charge analysis support the above mentioned AIM and NBO results very well. The results are shown in figure 2.23 and table 2.16.

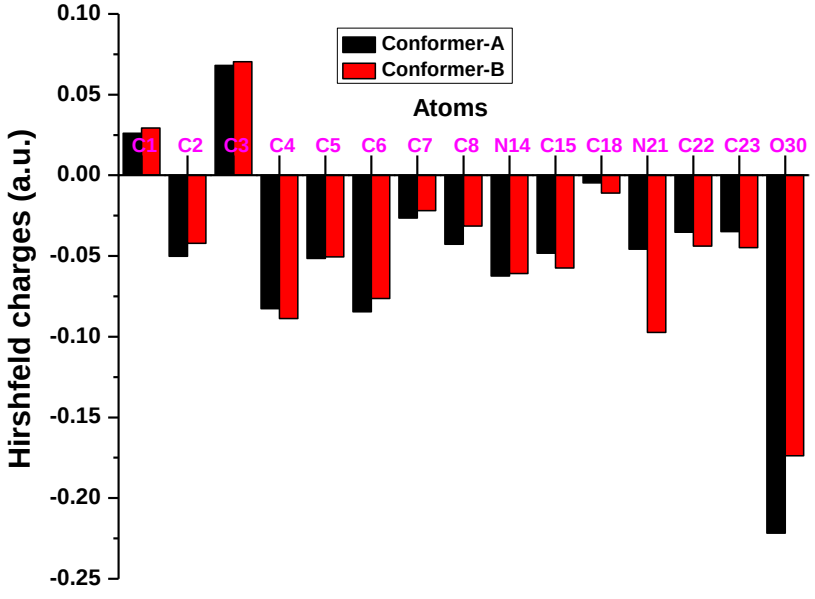

Figure 2.23: Charge distribution plot of Hirshfeld charges for conformer-A and B ; the number after atoms represent the label of that atom shown in figure 2.7

From figure 2.23 it is inferred that both conformers differed significantly in charge values only for few atoms of psilocin molecule. For instance O30 atom has more negative charge and H31 atom has less positive charge in conformer-A than conformer-B. Similarly the N21 atom has less negative charge in A-conformer than B. These observation suggests that due to H-bond formation between N21----H31-O30 in A-conformer the charge values differ significantly than B-conformer where no such H-bond formation was observed. Whereas, in conformer-B there is less negative charge on O30 and less positive charge on H20 and H17 which further suggest the weak H-bond interaction between O30 and H20, H17 atoms.

Table 2.16: The Hirshefield charge values (a.u.) on each atom of both the conformers (A & B) of psilocin molecule

Atoms	Hirshfeld charges [a.u.]	
	Conformer-A	Conformer-B
C1	0.025	0.029
C2	-0.050	-0.042
C3	0.068	0.070
C4	-0.082	-0.088
C5	-0.051	-0.050
C6	-0.084	-0.076
C7	-0.026	-0.021
C8	-0.042	-0.031
H9	0.032	0.030
H10	0.034	0.036
H11	0.030	0.034
H12	0.138	0.139
H13	0.042	0.045
N14	-0.062	-0.060
C15	-0.048	-0.057
H16	0.032	0.025
H17	0.031	0.027
C18	-0.004	-0.011
H19	0.020	0.022
H20	0.032	0.024
N21	-0.045	-0.097
C22	-0.035	-0.044
C23	-0.034	-0.044
H24	0.038	0.032
H25	0.041	0.028
H26	0.023	0.014
H27	0.039	0.031
H28	0.023	0.012
H29	0.039	0.029
O30	-0.222	-0.173
H31	0.095	0.168

[Note]: numbers after atom represent label of that atom (figure 2.7)

2.3.7c Charge analysis of mescaline

ESP[MK(Merz Kollman)] charge calculation at the CCSD/cc-pVDZ level of theory was performed to understand how the aforementioned intramolecular non-covalent interactions affect the charges on each atom of mescaline. ESP[MK] charge plot, shown

in figure 2.24, reveals that in conformer-M6, the charge on N15 is relatively lower compared to the M1 conformer. The N-H---π interaction that exists in conformer-M6 is the cause of this discrepancy. Similarly, H17 exhibits a slightly more positive charge than H16 due to the same interaction. On the other hand, O19 displays a reduced negative charge as its lone pair of electrons is donated to an adjacent C-H antibonding orbital. These factors contribute to the stability of M6. Additionally, Hirshfeld charge calculations were conducted for both conformers, and the results closely aligned with the findings from the ESP charge calculation. The charge distribution curve of Hirshfeld charge calculation is shown in figure 2.25 and the charge value on each atom are given in table 2.17.

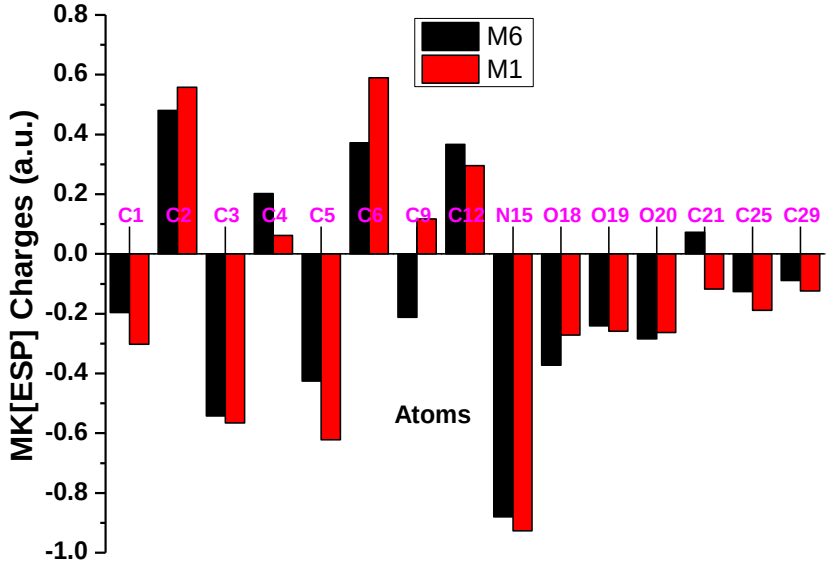

Figure 2.24: Charge distribution plot of ESP[MK] charges for conformer-M6 and conformer-M1 ; the number after atoms represent the label of that atom shown in figure 2.12

Table 2.17: The ESP[MK] and Hirshefield charge values (a.u.) on each atom of both the conformers (M6 & M1) of mescaline at CCSD/cc-pVDZ level of theory

No.	Atoms	Charge Values [a.u.]			
		Conformer-M6		Conformer-M1	
		ESP[MK]	Hirshfeld	ESP[MK]	Hirshfeld
1	C	-0.196	0.0487	-0.303	0.044
2	C	0.480	0.0916	0.558	0.094
3	C	-0.542	-0.077	-0.565	-0.089
4	C	0.202	0.011	0.061	0.014
5	C	-0.425	-0.072	-0.622	-0.087
6	C	0.372	0.084	0.590	0.094
7	H	0.214	0.033	0.223	0.027
8	H	0.207	0.035	0.244	0.029
9	C	-0.212	-0.031	0.117	-0.032
10	H	0.102	0.026	0.011	0.021
11	H	0.048	0.025	0.019	0.026
12	C	0.366	0.016	0.295	0.015
13	H	-0.060	0.008	-0.053	0.007
14	H	-0.0004	0.023	0.023	0.020
15	N	-0.879	-0.227	-0.926	-0.225
16	H	0.320	0.093	0.342	0.094
17	H	0.324	0.083	0.323	0.090
18	O	-0.372	-0.198	-0.271	-0.173
19	O	-0.240	-0.190	-0.258	-0.196
20	O	-0.284	-0.175	-0.26	-0.173
21	C	0.072	0.033	-0.117	0.040
22	H	0.059	0.029	0.082	0.029
23	H	0.059	0.036	0.108	0.042
24	H	0.032	0.024	0.079	0.030
25	C	-0.126	0.034	-0.188	0.032
26	H	0.108	0.0272	0.104	0.023
27	H	0.106	0.036	0.131	0.035
28	H	0.086	0.026	0.104	0.023
29	C	-0.088	0.040	-0.124	0.039
30	H	0.086	0.031	0.084	0.029
31	H	0.097	0.042	0.108	0.042
32	H	0.080	0.032	0.081	0.028

[Note]: numbers after atom represent label of that atom (figure 2.12)

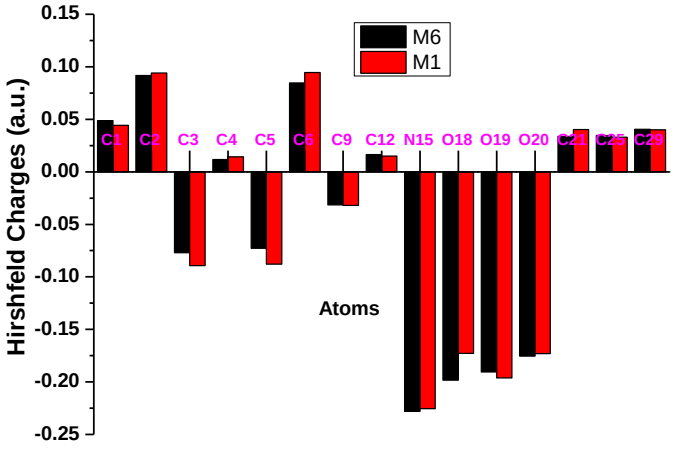

Figure 2.25: Charge distribution plot of Hirshfeld charges for conformer-M6 and M1 ; the number after atoms represent the label of that atom shown in article, figure 2.12

2.3.8a Electrostatic potential maps (MEPs) of psilocybin

The nucleophilic and electrophilic centers in psilocybin were found out with the help of ESP MEP and depicted in figure 2.26. The colour scale indicates red as minimum electrostatic potential which means there is excess of electrons or loosely bound electrons therefore this region is prone to electrophilic attack and blue as the maximum of electrostatic potential acts opposite and therefore prone to nucleophilic attack. From the analysis of ESP maps it was observed that the negative potential was located over the P=O group in both the conformers therefore this is prone to electrophilic attack while the positive electrostatic potential is located only on N-H of indole in both the conformers, rendering it prone to nucleophilic attack.

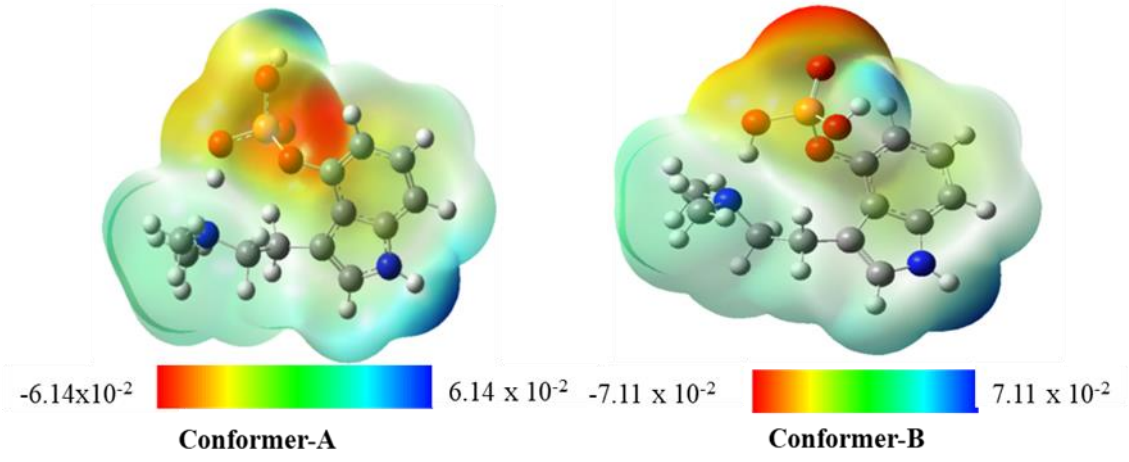

Figure 2.26: ESP map on optimized geometries of both the conformers (A & B) of psilocybin

2.3.8b Electrostatic potential maps (MEPs) of psilocin

The ESP maps of psilocin revealed that the negative potential was located over OH moiety and positive electrostatic potential is located on N-H of indole ring in case of conformer-A. In conformer-B the negative potential was located over N21 of alkyl amino group while positive electrostatic potential was located on N-H of indole ring. The ESP maps of the conformers (A and B) are shown in figure 2.27.

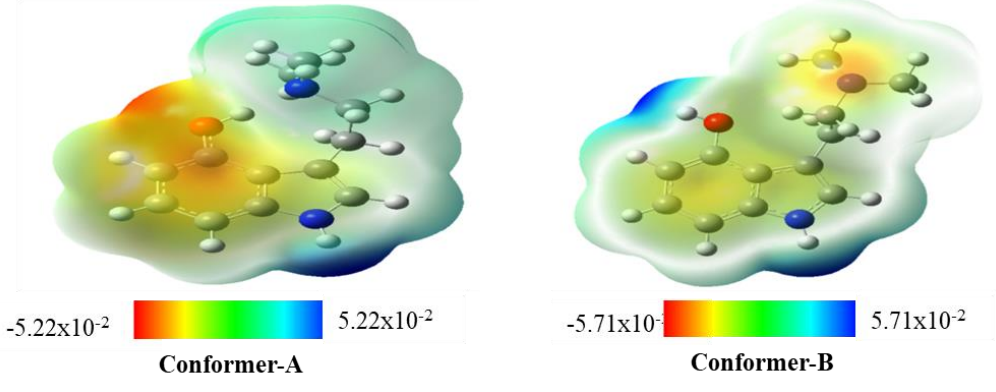

Figure 2.27: ESP map on optimized geometries of both conformers (A and B) of psilocin molecule

2.3.8c Electrostatic potential maps (MEPs) of mescaline

The optimized structures of two mescaline conformers (M6 and M1) were subjected to ESP mapping to determine their positive and negative electrostatic potentials, as shown in figure 2.28. It was observed that in both the conformers (M6 and M1) the negative potential was located over all oxygen atoms while positive potential was located over the N-H moiety of mescaline.

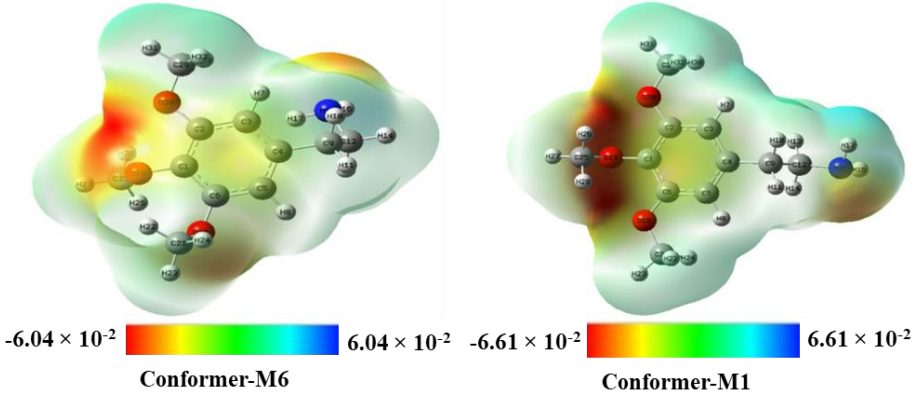

Figure 2.28: ESP map on optimized geometries of both the conformers (M6 & M1) of mescaline

2.3.9a Spectroscopic analysis of psilocybin

UV-visible spectrum of psilocybin was computed using TD-DFT method and the result is shown in Figure 2.29 where the λ_{max} of both the conformers A and B appear at 266 nm and 265 nm, respectively which matches well with the experimental data reported in literature.[69,70]

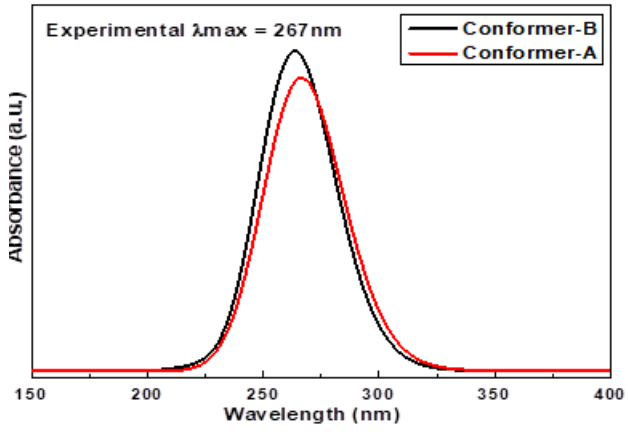

Figure 2.29: Calculated UV spectrum of conformer-A (λ_{max} = 266 nm) and conformer-B (λ_{max} = 265 nm) of psilocybin

^{1}H NMR spectrum was also calculated using GIAO method and the peaks are in good agreement with the literature.[71] In the experiment ^{1}H NMR peaks were observed in CD_3OD with TSP while in our simulated ^{1}H NMR the methanol solution with TMS was utilized. Experimentally observed and simulated ^{1}H NMR peaks are compared in table 2.18.

Table 2.18: Comparison of experimental and simulated 1H NMR peaks of psilocybin at B3LYP/cc-pVTZ level of theory

^{1}H NMR peaks [ppm]			Assignment[#]
Reported in literature[71] [in CD_3OD with TSP], δ	Simulated peaks, δ [in CH_3OH with TMS]		
	Conformer-A	Conformer-B	
7.02	7.28	7.54	Benzene H, m
3.30	3.37	3.28	4H, m
2.86	2.66	2.61	6H, s

[#]: s and m denote multiplicity of the peaks namely singlet and multiplet respectively.

The vibrational spectroscopic study was done for the assignment of functional groups present in psilocybin. Psilocybin consists of 36 atoms, which has 102 normal modes of vibrations. This molecule belongs to the C1 symmetry point group. The selective calculated IR active vibrational modes and their respective experimental IR frequencies

of both the conformers are shown in table 2.19 along with their tentative assignments. The calculated vibrational modes were found in good agreement with literature data.[71]

In literature, the spectroscopic data available for psilocybin is not conformer specific. But computationally it was observed that this molecule has many conformers. So it was assumed that the spectroscopic data reported in literature is an ensemble of many conformers. Yet the predictions reported herein for the two conformers matched exceedingly well with the experimental observations.

Table 2.19: Calculated and experimental IR vibrational frequencies of psilocybin at B3LYP/cc-pVTZ level of theory

Calculated wave numbers [cm^{-1}]		Experimental wave numbers [cm^{-1}][71]	Tentative assignment of vibrations[##]
Conformer-A	Conformer-B		
465.30	458.99	461.25	ω_{PO4}breathing vibration
742.76	757.44	746.77	$\delta_{CCC(indole)} + \nu_{NR2} + \omega_{CH}$(indole)
800.45	796.96	785.93	ρ_{CH2}
864.74	856.24	855.21	$\delta_{CCC(indole)}+\nu_{P-OH}$
907.99	902.15	920.69	ν_{P-OH}
1060.79	1045.34	1042.33	ρ_{OH}
1106.40	1101.71	1101.24	$\rho_{CH(indole)} + \rho_{CH2}$
1243.01	1231.67	1229.69	$\delta_{CCC} + \nu_{C=N}$(indole)
1299.56	1350.06	1348.55	$\nu_{P=O} + \rho_{CH2}$
1441.36	1442.23	1442.19	$\nu_{C=C} + \nu_{C=N}$(indole)
1503.73	1506.35	1503.84	δsCH_3
3185.08	3170.91	3179.96	$\nu_{CH(benzene)}$

[##]: Note: ω=wagging, δ=bending, ν=stretching, and ρ=rocking (in plane).

2.3.9b Spectroscopic analysis of psilocin

For psilocin also UV-visible spectrum was computed using TD-DFT method and the result was found in good agreement with the experimental data reported in literature.[69–71] As in literature the spectrum was recorded in methanol solution therefore the calculation for UV-visible spectrum was performed using methanol solvent utilizing implicit solvation model[72] based on density under default setting in Gaussian 16 package. The peaks (nm) reported in literature were 222.5, 268.0, 284.5 whereas, for conformer-

A, the peaks (nm) were predicted at 221.5, 252.3, 271.1, and for Conformer-B at 229.1, 256.9, 277.5.

^{1}H-NMR spectrum was also calculated using GIAO method and the peaks are in good agreement with the literature.[71] The results are compared with reported peaks and shown in table 2.20.

Table 2.20: Comparison of experimental and simulated ^{1}H-NMR peaks of psilocin at B3LYP/cc-pVTZ level of theory

^{1}H NMR peaks [ppm]			Assignment[#]
Reported in literature[71] [in CD_3OD with TSP], δ	Simulated peaks, δ [in CH_3OH with TMS		
	Conformer-A	Conformer-B	
6.86	7.37	7.04	1H, dd
6.33	6.93	6.94	1H, d
6.31	6.88	6.49	1H, d
3.30	3.32	3.47	4H, m
3.00	2.99	2.81	2H, m
2.72	2.66	2.76	2H, m
2.34	2.45	2.53	6H, s

[#]: s, d and m denote multiplicity of the peaks namely singlet, doublet and multiplet respectively.

The normal modes of vibration of psilocin was calculated and assigned which is summarized in table 2.21. The calculated vibrational modes were found in good agreement with literature data.[71]

Table 2.21: Calculated and experimental IR vibrational frequencies of psilocin molecule at B3LYP/cc-pVTZ level of theory

Calculated wave numbers [cm^{-1}]		Experimental wave numbers [cm^{-1}][71]	Tentative assignment of vibrations[##]
Conformer A	Conformer B		
412.74	421.69	427.91	$\omega_{(N\text{-}(CH3)3}$
489.92	498.68	479.76	$\delta_{(ccc)}$ (Benzene ring of indole)
547.56	547.67	545.46	$\omega_{(ccc)}$ (indole ring)
594.33	598.28	590.27	$\delta_{(ccc)}$ (indole)

634.92	621.83	613.22	$\omega_{(ccc)}$ (Benzene ring of indole)
659.61	675.45	686.14	$\nu_{s(indole)}$ ring breathing vibration
724.16	736.56	725.47	$\nu_{as(indole)}$
788.44	774.78	769.45	$\nu_{s\ (N21-C)}$
849.43	838.78	832.87	$\delta_{(ccc)}$ (indole)
963.60	991.57	995.19	$\rho_{CH2} + \rho_{N14CC}$
1031.72	1029.31	1034.92	$\nu_{as\ (N21-C)}$
1172.69	1177.75	1174.88	$\tau_{CH2}+\tau_{CH3}+\delta_{CH(indole)}$
1236.61	1226.40	1232.37	$\delta_{CH(indole)}$
1253.66	1255.87	1254.81	$\delta_{CH(indole)} + \delta_{OH} + \tau_{CH2}$
1356.56	1329.68	1341.97	$\nu_{(CC)(indole)}$
1386.82	1380.05	1384.74	ω_{CH2}
1444.92	1443.67	1441.75	ω_{CH3}
1469.47	1478.88	1470.48	δ_{sCH2}, δ_{sCH3}
1583.92	1584.66	1588.21	ν_{aC-C} (Indole ring)
-	-	2325.12	-
2957.78	2919.38	2958.84	ν_{C-H} (methyl)
3236.14	3240.05	3280.82	ν_{C-H} (5 membered ring of indole)

[##]: δ = in plane bending, δ_s=in plane scissoring, ω= out of plane wagging, τ= out of plane twisting, ρ= in plane rocking, ν= stretching, ν_s= symmetric stretching, ν_{as}= asymmetric stretching

2.3.9c Spectroscopic analysis of mescaline

Mescaline's UV-visible spectrum was calculated using the TD-DFT method, and it turned out that the results were in extremely good agreement with the experimental findings that had been published in the literature.[73,74] In the literature, the reported λmax (nm) was 269 nm, while the calculated λmax (nm) for both conformers was observed at 267-268 nm. Notably, the UV-visible spectrum calculation utilized the optimized geometry of both conformers (M1 and M6) at CCSD/cc-pVDZ level, followed by re-optimization at B3LYP/cc-pVTZ level utilizing the TD-DFT method.

The 1H-NMR spectrum was computed using the GIAO method, and a favorable agreement with the literature was observed.[73] The results are compared with reported peaks and shown in table 2.22.

Table 2.22: Comparison of experimental and simulated ^{1}H-NMR peaks of mescaline at B3LYP/cc-pVTZCCSD/cc-pVDZ level of theory

^{1}H NMR peaks [ppm]			Assignment[#]
Reported in literature[73] [in DMSO-d6], δ	Simulated peaks[in DMSO], δ		
	Conformer-M6	Conformer-M1	
6.52	6.8	6.7	2H, s
3.76	3.6	3.9	6H, s
3.62	3.8	3.7	3H, s
2.65-2.68	2.7	2.7	2H, t
2.88-2.91	3.0	2.8	2H, t

[#]: s, and t denote multiplicity of the peaks namely singlet and triplet respectively.

The harmonic normal modes of mescaline were computed at B3LYP/cc-pVTZ//CCSD/cc-pVDZ theoretical level, considering its point group as C1. Table 2.23 displays the selectively computed IR-active vibrational modes and their corresponding experimental IR vibrational modes for conformer-M6 and M1, along with a tentative assignment of the modes. The computed vibrational modes exhibit favorable agreement with the literature data.[73]

Table 2.23: Calculated and experimental IR vibrational frequencies of mescaline at B3LYP/cc-pVTZ//CCSD/cc-pVDZ level of theory

Calculated normal modes of vibrations of mescaline [cm^{-1}]		Experimentally reported normal modes of vibrations of mescaline [cm^{-1}] [73]	Tentative assignment [##]
Conformer-M6	Conformer-M1		
3488	3483	3437	ν_{N-H}
2950	2953	2943	ν_{C-H}
1653	1656	1633	$\delta_{(NH2)}$
1513	1519	1514	$\delta_{s(CH3)}$
1134	1166	1128	ν_{C-O}
985	997	995	δ_{CH} (benzene ring)
847	849	831	ω_{CH} (benzene ring)
638	617	619	τ_{CH} (benzene ring)

[##]: ν= stretching, δ = in plane bending, δ_s=in plane scissoring, ω= out of plane wagging, τ= out of plane twisting

2.4 Conclusion

The conformational space of psilocybin has several local minima and among them, the lowest energy conformer, identified as conformer-A, along with another conformer were taken up for detailed analysis. The difference of energy between these two conformers is about 2.08 kcal/mol. The calculated HOMO-LUMO gap for both the conformers suggest the chemical activity of this molecule. Through NBO analysis it was observed that the intramolecular n→π* and π→π* charge transfers and hyper conjugative interactions are responsible for the stability of psilocybin. Also by the analysis of AIM calculation it was observed that it is the strong intramolecular H-bond formation between N21 and H36 atom in both conformers A and B which provides stability to this molecule. In the UV visible spectrum the λmax observed at 266 nm for conformer-A exactly matched with the reported experimental value. The proton NMR peaks too were found in good agreement. Similarly the assignment of harmonic vibrational frequency modes was done by means of DFT calculation for both the conformers of psilocybin for the very first time and it agreed with experimentally reported vibrational modes exceedingly well. Psilocybin consists of attractive electrophilic and nucleophilic centers which make it a very chemically active molecule. These results and observations indicate that both the conformers of psilocybin are similar in properties having only 2.08 kcal/mol difference in energy between them. And these are stable due to intramolecular charge transfers including n→π* and π→π* charge transfers, hyper conjugative interactions and intramolecular H-bond interaction. These are in accordance with the earlier reported crystal structure of psilocybin where two conformers were observed. Although, from this detailed computational analysis of psilocybin, conformer-A was found to be the most dominating conformer.

In a similar manner, the conformational space of psilocin molecule was extensively explored by scanning various dihedral angles and two low lying conformers were taken up for detailed analysis. The second conformer was found 5.4 kcal/mol higher in energy compared to the most stable conformer. Dimers of these two conformers showed dissimilar interaction patterns. Whereas in conformer-A (global minimum) the

intramolecular H-bonding dominated intermolecular interaction, the opposite was observed in conformer-B which is in accordance with the past reports from X-ray crystal structure studies of psilocin. Although intramolecular H-bond interactions for dimers of conformer-A was conjectured earlier the calculations reported herein validates the conjecture for the very first time and provide a definite path for future experiments.

Likewise, Mescaline's conformational space contains multiple local minima, and two of them, namely conformer-M6 (the global minium) and conformer-M1, were selected for in-depth analysis. At the CCSD/cc-pVDZ level, these two conformers have an energy difference of 1.5 kcal/mol. The computed HOMO-LUMO gap for both conformers offers valuable insights into the chemical reactivity of mescaline. As per to the NBO analysis, the molecule's stability is aided by the n→π* and π→π* intramolecular charge transfers, along with hyperconjugative electron delocalization. Additionally, the AIM calculation highlights the significance of a robust intramolecular NH---π interaction in conformer M6, which enhances the stability of this specific conformation. The calculated geometrical parameters and predicted structure of M6 exhibit excellent agreement with previously reported conformers obtained from X-ray studies of mescaline. The UV-visible spectrum reveals a significant match in λmax at 267 nm for both conformer-M6 and M1, closely resembling the experimental values. Similar to this, there is good agreement between anticipated peak positions in the proton NMR spectrum and the results from experiments. Moreover, the computed normal modes of vibration highly correspond to the experimentally reported vibrational modes found in the literature. Also, there are appealing nucleophilic and electrophilic centers exist in mescaline, making it a highly reactive compound. Among the conformers, M6 stands out as the most stable and abundant due to its intramolecular NH---π interaction. While the second most stable conformer is only 1.5 kcal/mol higher in energy, both conformers exhibit similar properties and stability attributed to π→π* and n→π* intramolecular charge transfers, as well as hyperconjugative interactions. These findings align with the previously reported crystal structures of mescaline.

2.5 References

(1) Cody, J. T. Hallucinogens. In *Handbook of Analytical Separations*; Elsevier, 2008; Vol. 6, pp 175–201.

(2) Derosa, G.; Maffioli, P. Alkaloids in the Nature: Pharmacological Applications in Clinical Practice of Berberine and Mate Tea. *Curr. Top. Med. Chem.* **2014**, *14* (2), 200–206.

(3) Tylš, F.; Páleníček, T.; Horáček, J. Psilocybin–Summary of Knowledge and New Perspectives. *Eur. Neuropsychopharmacol.* **2014**, *24* (3), 342–356.

(4) Hofmann, A.; Heim, R.; Brack, A.; Kobel, H. Psilocybin, a Psychotropic Compound from the Mexican Intoxicant Psilocybe Mexicana Heim. *Experience* **1958**, *14*, 107–109.

(5) Tittarelli, R.; Mannocchi, G.; Pantano, F.; Saverio Romolo, F. Recreational Use, Analysis and Toxicity of Tryptamines. *Curr. Neuropharmacol.* **2015**, *13* (1), 26–46.

(6) Bhadoria, P.; Ramanathan, V. Conformational Landscape and Properties of Psilocybin: A Computational Approach. *ChemistrySelect* **2022**, *7* (37), e202203026.

(7) Inserra, A.; De Gregorio, D.; Gobbi, G. Psychedelics in Psychiatry: Neuroplastic, Immunomodulatory, and Neurotransmitter Mechanisms. *Pharmacol. Rev.* **2021**, *73* (1), 202–277.

(8) Strassman, R. Human Hallucinogen Interactions with Drugs Affecting Serotonergic. *Neuropsychopharmacology* **1992**, *7* (3).

(9) Vollenweider, F. X.; Vollenweider-Scherpenhuyzen, M. F.; Bäbler, A.; Vogel, H.; Hell, D. Psilocybin Induces Schizophrenia-like Psychosis in Humans via a Serotonin-2 Agonist Action. *Neuroreport* **1998**, *9* (17), 3897–3902.

(10) Soper, R. S. Massospora Levispora, a New Species of Fungus Pathogenic to the Cicada, Okanagana Rimosa. *Can. J. Bot.* **1963**, *41* (6), 875–878.

(11) Soper, S. The Genus Massospora, Entomopathogenic for Cicadas. Part I. Taxonomy of the Genus. *Mycotaxon* **1974**, *1*, 13–40.

(12) White, J. A.; Ganter, P.; McFarland, R.; Stanton, N.; Lloyd, M. Spontaneous, Field Tested and Tethered Flight in Healthy and Infected Magicicada Septendecim L. *Oecologia* **1983**, *57*, 281–286.

(13) Cooley, J. R.; Marshall, D. C.; Hill, K. B. A Specialized Fungal Parasite (Massospora Cicadina) Hijacks the Sexual Signals of Periodical Cicadas (Hemiptera: Cicadidae: Magicicada). *Sci. Rep.* **2018**, *8* (1), 1432.

(14) Murphy, J. M.; Redden, G. A. Fungal Infection and Gender Confusion in the Wing-Banger Cicada Platypedia Putnami. *Norse Sci. NKU* **2003**, *65*.

(15) Petcher, T. J.; Weber, H. P. Crystal Structures of the Teonanácatl Hallucinogens. Part II. Psilocin, C 12 H 15 N 2 O. *J. Chem. Soc. Perkin Trans. 2* **1974**, No. 8, 946–948.

(16) Horita, A. Some Biochemical Studies on Psilocybin and Psilocin. *J Neuropsychiatry* **1963**, *4*, 270–273.

(17) McKenna, D. J.; Repke, D. B.; Lo, L.; Peroutka, S. J. Differential Interactions of Indolealkylamines with 5-Hydroxytryptamine Receptor Subtypes. *Neuropharmacology* **1990**, *29* (3), 193–198.

(18) Vollenweider, F. X.; Vollenweider-Scherpenhuyzen, M. F.; Bäbler, A.; Vogel, H.; Hell, D. Psilocybin Induces Schizophrenia-like Psychosis in Humans via a Serotonin-2 Agonist Action. *Neuroreport* **1998**, *9* (17), 3897–3902.

(19) González-Maeso, J.; Weisstaub, N. V.; Zhou, M.; Chan, P.; Ivic, L.; Ang, R.; Lira, A.; Bradley-Moore, M.; Ge, Y.; Zhou, Q.; others. Hallucinogens Recruit Specific Cortical 5-HT2A Receptor-Mediated Signaling Pathways to Affect Behavior. *Neuron* **2007**, *53* (3), 439–452.

(20) Kometer, M.; Schmidt, A.; Bachmann, R.; Studerus, E.; Seifritz, E.; Vollenweider, F. X. Psilocybin Biases Facial Recognition, Goal-Directed Behavior, and Mood State toward Positive Relative to Negative Emotions through Different Serotonergic Subreceptors. *Biol. Psychiatry* **2012**, *72* (11), 898–906.

(21) Carhart-Harris, R. L.; Bolstridge, M.; Day, C. M.; Rucker, J.; Watts, R.; Erritzoe, D. E.; Kaelen, M.; Giribaldi, B.; Bloomfield, M.; Pilling, S.; others. Psilocybin

with Psychological Support for Treatment-Resistant Depression: Six-Month Follow-Up. *Psychopharmacology (Berl.)* **2018**, *235*, 399–408.

(22) Carhart-Harris, R. L.; Bolstridge, M.; Rucker, J.; Day, C. M.; Erritzoe, D.; Kaelen, M.; Bloomfield, M.; Rickard, J. A.; Forbes, B.; Feilding, A.; others. Psilocybin with Psychological Support for Treatment-Resistant Depression: An Open-Label Feasibility Study. *Lancet Psychiatry* **2016**, *3* (7), 619–627.

(23) Moreno, F. A.; Wiegand, C. B.; Taitano, E. K.; Delgado, P. L. Safety, Tolerability, and Efficacy of Psilocybin in 9 Patients with Obsessive-Compulsive Disorder. *J. Clin. Psychiatry* **2006**, *67* (11), 1735–1740.

(24) Griffiths, R. R.; Johnson, M. W.; Carducci, M. A.; Umbricht, A.; Richards, W. A.; Richards, B. D.; Cosimano, M. P.; Klinedinst, M. A. Psilocybin Produces Substantial and Sustained Decreases in Depression and Anxiety in Patients with Life-Threatening Cancer: A Randomized Double-Blind Trial. *J. Psychopharmacol. (Oxf.)* **2016**, *30* (12), 1181–1197.

(25) Ross, S.; Bossis, A.; Guss, J.; Agin-Liebes, G.; Malone, T.; Cohen, B.; Mennenga, S. E.; Belser, A.; Kalliontzi, K.; Babb, J.; others. Rapid and Sustained Symptom Reduction Following Psilocybin Treatment for Anxiety and Depression in Patients with Life-Threatening Cancer: A Randomized Controlled Trial. *J. Psychopharmacol. (Oxf.)* **2016**, *30* (12), 1165–1180.

(26) Bogenschutz, M. P.; Forcehimes, A. A.; Pommy, J. A.; Wilcox, C. E.; Barbosa, P. C.; Strassman, R. J. Psilocybin-Assisted Treatment for Alcohol Dependence: A Proof-of-Concept Study. *J. Psychopharmacol. (Oxf.)* **2015**, *29* (3), 289–299.

(27) Johnson, M. W.; Garcia-Romeu, A.; Cosimano, M. P.; Griffiths, R. R. Pilot Study of the 5-HT2AR Agonist Psilocybin in the Treatment of Tobacco Addiction. *J. Psychopharmacol. (Oxf.)* **2014**, *28* (11), 983–992.

(28) Sherwood, A. M.; Kargbo, R. B.; Kaylo, K. W.; Cozzi, N. V.; Meisenheimer, P.; Kaduk, J. A. Psilocybin: Crystal Structure Solutions Enable Phase Analysis of Prior Art and Recently Patented Examples. *Acta Crystallogr. Sect. C Struct. Chem.* **2022**, *78* (1), 36–55.

(29) Chothia, C.; Pauling, P. On the Conformations of Hallucinogenic Molecules and Their Correlation. *Proc. Natl. Acad. Sci.* **1969**, *63* (4), 1063–1070.

(30) Halberstadt, A. L.; Geyer, M. A. Serotonergic Hallucinogens as Translational Models Relevant to Schizophrenia. *Int. J. Neuropsychopharmacol.* **2013**, *16* (10), 2165–2180.

(31) Monte, A. P.; Waldman, S. R.; Marona-Lewicka, D.; Wainscott, D. B.; Nelson, D. L.; Sanders-Bush, E.; Nichols, D. E. Dihydrobenzofuran Analogues of Hallucinogens. 4. Mescaline Derivatives. *J. Med. Chem.* **1997**, *40* (19), 2997–3008.

(32) Nelson, D.; Lucaites, V.; Wainscott, D.; Glennon, R. Comparisons of Hallucinogenic Phenylisopropylamine Binding Affinities at Cloned Human 5-HT2A, 5-HT2B and 5-HT2C Receptors. *Naunyn. Schmiedebergs Arch. Pharmacol.* **1999**, *359*, 1–6.

(33) Davis, W.; Bedford, J.; Buelke, J.; Guinn, M.; Hatoum, H.; Waters, I.; Wilson, M.; Braude, M. Acute Toxicity and Gross Behavioral Effects of Amphetamine, Four Methoxyamphetamines, and Mescaline in Rodents, Dogs, and Monkeys. *Toxicol. Appl. Pharmacol.* **1978**, *45* (1), 49–62.

(34) Ogunbodede, O.; McCombs, D.; Trout, K.; Daley, P.; Terry, M. New Mescaline Concentrations from 14 Taxa/Cultivars of Echinopsis Spp.(Cactaceae)("San Pedro") and Their Relevance to Shamanic Practice. *J. Ethnopharmacol.* **2010**, *131* (2), 356–362.

(35) Cassels, B. K.; Sáez-Briones, P. Dark Classics in Chemical Neuroscience: Mescaline. *ACS Chem. Neurosci.* **2018**, *9* (10), 2448–2458.

(36) Clement, B. A.; Goff, C. M.; Forbes, T. D. A. Toxic Amines and Alkaloids from Acacia Berlandieri. *Phytochemistry* **1997**, *46* (2), 249–254.

(37) Bruhn, J. G.; De Smet, P. A.; El-Seedi, H. R.; Beck, O. Mescaline Use for 5700 Years. *The Lancet* **2002**, *359* (9320), 1866.

(38) El-Seedi, H. R.; De Smet, P. A.; Beck, O.; Possnert, G.; Bruhn, J. G. Prehistoric Peyote Use: Alkaloid Analysis and Radiocarbon Dating of Archaeological

Specimens of Lophophora from Texas. *J. Ethnopharmacol.* **2005**, *101* (1–3), 238–242.

(39) Halpern, J. H.; Sherwood, A. R.; Hudson, J. I.; Yurgelun-Todd, D.; Pope Jr, H. G. Psychological and Cognitive Effects of Long-Term Peyote Use among Native Americans. *Biol. Psychiatry* **2005**, *58* (8), 624–631.

(40) Carstairs, S. D.; Cantrell, F. L. Peyote and Mescaline Exposures: A 12-Year Review of a Statewide Poison Center Database. *Clin. Toxicol.* **2010**, *48* (4), 350–353.

(41) Heffter, A. Ueber Cacteenalkaloide. *Berichte Dtsch. Chem. Ges.* **1896**, *29* (1), 216–227.

(42) Spaeth, E. Ueber DieAnhalonium-Alkaloide. *Monatshefte Fuer Chem.* **1919**, *40* (2), 129–154.

(43) Rickli, A.; Moning, O. D.; Hoener, M. C.; Liechti, M. E. Receptor Interaction Profiles of Novel Psychoactive Tryptamines Compared with Classic Hallucinogens. *Eur. Neuropsychopharmacol.* **2016**, *26* (8), 1327–1337.

(44) Agin-Liebes, G.; Haas, T. F.; Lancelotta, R.; Uthaug, M. V.; Ramaekers, J. G.; Davis, A. K. Naturalistic Use of Mescaline Is Associated with Self-Reported Psychiatric Improvements and Enduring Positive Life Changes. *ACS Pharmacol. Transl. Sci.* **2021**, *4* (2), 543–552.

(45) Vamvakopoulou, I. A.; Narine, K. A.; Campbell, I.; Dyck, J. R.; Nutt, D. J. Mescaline: The Forgotten Psychedelic. *Neuropharmacology* **2022**, 109294.

(46) Taurian, O.; Contreras, R. Interactions That Define the Alkylamine Side-Chain Conformation in Phenylalkylamine Hallucinogens: An Ab Initio Study. *J. Mol. Struct. THEOCHEM* **2000**, *504* (1–3), 119–126.

(47) Becker, O. M.; MacKerell Jr, A. D.; Roux, B.; Watanabe, M. *Computational Biochemistry and Biophysics*; Crc Press, 2001.

(48) Mavromoustakos, T.; Zervou, M.; Zoumpoulakis, P.; Kyrikou, I.; Benetis, N.; Polevaya, L.; Roumelioti, P.; Giatas, N.; Zoga, A.; Minakakis, P. M. Conformation and Bioactivity. Design and Discovery of Novel Antihypertensive Drugs. *Curr. Top. Med. Chem.* **2004**, *4* (4), 385–401.

(49) Bochevarov, A. D.; Watson, M. A.; Greenwood, J. R.; Philipp, D. M. Multiconformation, Density Functional Theory-Based p K a Prediction in Application to Large, Flexible Organic Molecules with Diverse Functional Groups. *J. Chem. Theory Comput.* **2016**, *12* (12), 6001–6019.

(50) Cheng, G.-J.; Zhang, X.; Chung, L. W.; Xu, L.; Wu, Y.-D. Computational Organic Chemistry: Bridging Theory and Experiment in Establishing the Mechanisms of Chemical Reactions. *J. Am. Chem. Soc.* **2015**, *137* (5), 1706–1725.

(51) Durig, J. R.; Deeb, H.; Darkhalil, I. D.; Klaassen, J. J.; Gounev, T. K.; Ganguly, A. The R0 Structural Parameters, Conformational Stability, Barriers to Internal Rotation, and Vibrational Assignments for Trans and Gauche Ethanol. *J. Mol. Struct.* **2011**, *985* (2–3), 202–210.

(52) Runge, E.; Gross, E. K. Density-Functional Theory for Time-Dependent Systems. *Phys. Rev. Lett.* **1984**, *52* (12), 997.

(53) London, F. Théorie Quantique Des Courants Interatomiques Dans Les Combinaisons Aromatiques. *J Phys Radium* **1937**, *8* (10), 397–409.

(54) McWeeny, R. Perturbation Theory for the Fock-Dirac Density Matrix. *Phys. Rev.* **1962**, *126* (3), 1028.

(55) Ditchfield, R. Self-Consistent Perturbation Theory of Diamagnetism: I. A Gauge-Invariant LCAO Method for NMR Chemical Shifts. *Mol. Phys.* **1974**, *27* (4), 789–807.

(56) Wolinski, K.; Hinton, J. F.; Pulay, P. Efficient Implementation of the Gauge-Independent Atomic Orbital Method for NMR Chemical Shift Calculations. *J. Am. Chem. Soc.* **1990**, *112* (23), 8251–8260.

(57) Cheeseman, J. R.; Trucks, G. W.; Keith, T. A.; Frisch, M. J. A Comparison of Models for Calculating Nuclear Magnetic Resonance Shielding Tensors. *J. Chem. Phys.* **1996**, *104* (14), 5497–5509.

(58) Petcher, T. J.; Weber, H. P. Crystal Structures of the Teonanácatl Hallucinogens. Part II. Psilocin, C 12 H 15 N 2 O. *J. Chem. Soc. Perkin Trans. 2* **1974**, No. 8, 946–948.

(59) Ernst, S.; Cagle, F. Mescaline Hydrobromide. *Acta Crystallogr. B* **1973**, *29* (7), 1543–1546.

(60) Tsoucaris, D.; De Rango, C.; Tsoucaris, G.; Zelwer, C.; PARTHASARATHY, R. t; FE, C. 1 (2-AMINOETHYL) 3, 4, 5-TRIMETHOXY-BENZENE (MESCALINE) HYDROCHLORIDE, C11H18CLNO3. **1973**.

(61) Weber, H. P.; Petcher, T. J. Crystal Structures of the Teonanácatl Hallucinogens. Part I. Psilocybin C 12 H 17 N 2 O 4 P. *J. Chem. Soc. Perkin Trans. 2* **1974**, No. 8, 942–946.

(62) Horn, A. S.; Post, M. L.; Kennard, O.; di Sanseverino, L. R. A Crystallographic and Theoretical Study of the Conformation of DOET and Its Significance for the Hallucinogenic Amphetamines. *J. Pharm. Pharmacol.* **1975**, *27* (1), 13–17.

(63) Emamian, S.; Lu, T.; Kruse, H.; Emamian, H. Exploring Nature and Predicting Strength of Hydrogen Bonds: A Correlation Analysis between Atoms-in-Molecules Descriptors, Binding Energies, and Energy Components of Symmetry-Adapted Perturbation Theory. *J. Comput. Chem.* **2019**, *40* (32), 2868–2881.

(64) Espinosa, E.; Molins, E.; Lecomte, C. Hydrogen Bond Strengths Revealed by Topological Analyses of Experimentally Observed Electron Densities. *Chem. Phys. Lett.* **1998**, *285* (3–4), 170–173.

(65) Espinosa, E.; Molins, E.; Lecomte, C. Hydrogen Bond Strengths Revealed by Topological Analyses of Experimentally Observed Electron Densities. *Chem. Phys. Lett.* **1998**, *285* (3–4), 170–173.

(66) Godfrey, P. D.; Rodgers, F. M.; Brown, R. D. Theory versus Experiment in Jet Spectroscopy: Glycolic Acid. *J. Am. Chem. Soc.* **1997**, *119* (9), 2232–2239.

(67) Johnson, E. R.; Keinan, S.; Mori-Sánchez, P.; Contreras-García, J.; Cohen, A. J.; Yang, W. Revealing Noncovalent Interactions. *J. Am. Chem. Soc.* **2010**, *132* (18), 6498–6506.

(68) Singh, U. C.; Kollman, P. A. An Approach to Computing Electrostatic Charges for Molecules. *J. Comput. Chem.* **1984**, *5* (2), 129–145.

(69) Borner, S.; Brenneisen, R. Determination of Tryptamine Derivatives in Hallucinogenic Mushrooms Using High-Performance Liquid Chromatography with Photodiode Array Detection. *J. Chromatogr. A* **1987**, *408*, 402–408.

(70) Anastos, N.; Lewis, S. W.; Barnett, N. W.; Sims, D. N. The Determination of Psilocin and Psilocybin in Hallucinogenic Mushrooms by HPLC Utilizing a Dual Reagent Acidic Potassium Permanganate and Tris (2, 2′-Bipyridyl) Ruthenium (II) Chemiluminescence Detection System. *J. Forensic Sci.* **2006**, *51* (1), 45–51.

(71) Shirota, O.; Hakamata, W.; Goda, Y. Concise Large-Scale Synthesis of Psilocin and Psilocybin, Principal Hallucinogenic Constituents of "Magic Mushroom." *J. Nat. Prod.* **2003**, *66* (6), 885–887.

(72) Marenich, A. V.; Cramer, C. J.; Truhlar, D. G. Universal Solvation Model Based on Solute Electron Density and on a Continuum Model of the Solvent Defined by the Bulk Dielectric Constant and Atomic Surface Tensions. *J. Phys. Chem. B* **2009**, *113* (18), 6378–6396.

(73) Aguayo, P. A. B.; Pinedo, V. M. R. Phytochemical Study of Echinopsis Peruviana. *Rev. Soc. Quím. Perú* **2014**, *80* (3), 202–210.

(74) Salomon, K.; Bina, A. F. Ultraviolet Absorption Spectra of Mescaline Sulfate and β-Phenylethylamine Sulfate. *J. Am. Chem. Soc.* **1946**, *68* (11), 2403–2403.